8
Double wavevector encoding

It is a remarkable feature of nuclear spin magnetisation that coherences created by RF pulses can persist for times on the order of seconds, thus making possible controlled evolution under the various terms of the spin Hamiltonian. Therein lies the basis of multi-dimensional NMR, in which evolution prior to the detection of the NMR signal imparts amplitude and phase information, which may be analysed in terms of those precursor time intervals. This chapter and the next address multiple encoding as it relates to spin translational motion. In particular, the use of magnetic field gradient pulses allow one to derive information about diffusion, flow, or molecular displacement distributions directly. If two successive PGSE pairs are used, then depending on the directions of these pulses, successive displacements of the same molecule may be correlated by orientation, or simply by directional sign. In the latter case an 'opposed' pair of identical amplitude gradient pulses will leave a phase shift that depends only on the change of velocity between the separate encodings, This is the so-called 'compensated double PGSE' NMR experiment. Alternatively, the amplitudes of each pair might be independently varied and the resulting signal Fourier transformed in each independent dimension, to produce a 2-D plot of correlated displacement distributions, commonly labelled a velocity exchange or VEXSY experiment. Such multidimensional PGSE NMR methods will be discussed in detail in Chapter 9.

First, however, we focus our attention on the double PGSE NMR experiment. Simply doubling the $\mathbf{q}$ encoding step gives us access to quite new information, though care is needed to ensure that the chosen pulse sequence and phase cycle select the appropriately encoded magnetisation coherence. Double PGSE NMR has particularly powerful application in the study of complex flow, in revealing the velocity autocorrelation function, and, in a targeted superposition of experiments, the non-local dispersion tensor. But we will also see that double encoding produces interesting outcomes even when the translational dynamics are governed by Brownian motion. In the case where molecules experience restricted diffusion in locally anisotropic pores or domains, the echo attenuation will depend on the relative orientation of the gradient pulse pairs, thus characterising local anisotropy despite a globally random orientation distribution for the domains. As we will see, a critical factor concerns the length of time allowed between the PGSE NMR pulse pairs, the so-called 'mixing time', τ_m. If τ_m is short compared with the time to diffuse between boundaries, then diffusive diffraction behaviour is dramatically different from that experienced with single wavevector encoding—more pronounced, and more information rich.

Translational Dynamics and Magnetic Resonance, First Edition, Paul T. Callaghan, © Paul T. Callaghan 2011.
Published in 2011 by Oxford University Press.

8.1 Double PGSE NMR

8.1.1 The double scattering process

Figure 8.1(a) shows a schematic double PGSE NMR experiment with independent gradient pairs. The delay between the gradient pulse pairs is the mixing time, τ_m. In Chapter 5, the analogy between the PGSE NMR measurement and inelastic neutron scattering was outlined. In the latter, neutrons undergo a momentum transfer in which a small amount of energy is exchanged due to the motion of the scattering nucleus. Extending this analogy to the representation of double PGSE NMR as a double scattering process requires an extra leap of imagination. Nonetheless, the coherent nature of the NMR evolution, in which the same nucleus experiences two independent sets of phase shifts from successive PGSE pairs, $\mathbf{q}$ and $\mathbf{q}'$, demands that we picture the scattering analogy as shown in Fig. 8.1.

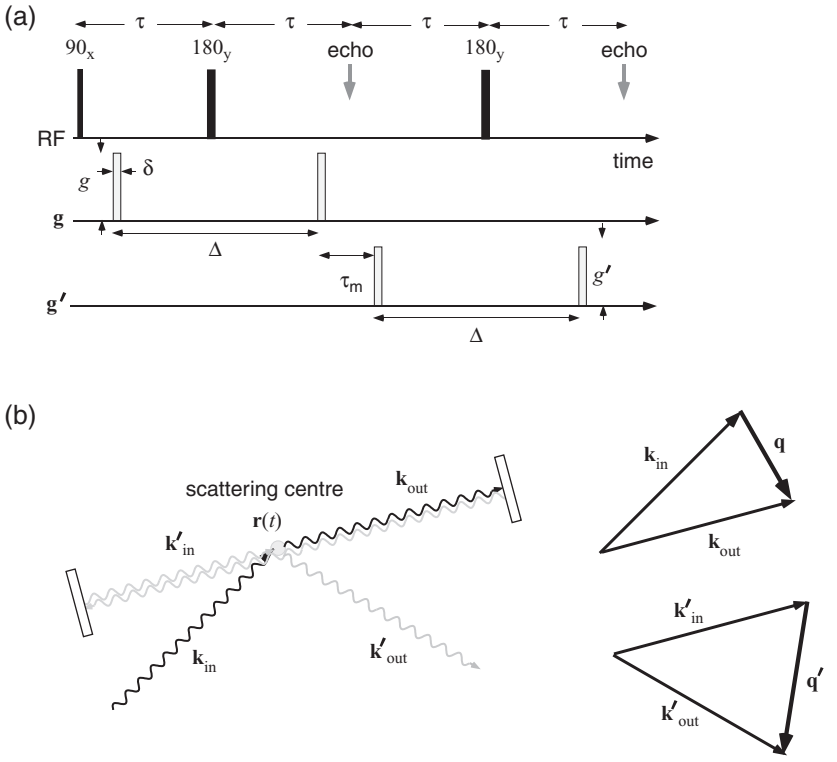

Fig. 8.1 (a) Schematic double PGSE sequence with independent gradients $\mathbf{g}'$ and $\mathbf{g}'$. The delay between the gradient pulse pairs is the mixing time, τ_m. (b) A somewhat implausible neutron scattering representation of double PGSE encoding, in which the scattered neutron is first reflected by mirrors (which define the initial emergence direction and hence $\mathbf{q}$) so as to return for a second scattering event, such that the final scattering vector is $\mathbf{q}'$, and defined by the direction of the detected neutron. The second scattering waves are shown in grey.

Here, the first scattered neutron is rerouted via mirrors to undergo a second scattering event, where judicious choice of path lengths could in principle be used to define τ_m. We know $\mathbf{q}$ by our choice of mirror arrangement, and we know $\mathbf{q}'$ by virtue of our detection of the emerging neutron. Of course, this picture is fanciful, especially given that the second scattering event must involve the original scattering centre, but it represents what we must do in order to make the inelastic neutron scattering experiment match the performance of double PGSE NMR. The very implausibility of such a scattering picture underscores the remarkable flexibility of PGSE NMR when it comes to tailored experimental design.

8.1.2 Compensated and uncompensated sequences

Spin-echo and stimulated-echo versions of the double PGSE NMR pulse sequence are shown in Fig. 8.2, along with their effective gradient equivalents. In these examples the second gradient pulse pair is chosen to be of exactly the same amplitude as the first, and applied along the same direction, or, as in the case of (c), in the same direction but with opposite sense. These particular versions of double PGSE NMR fall into a special class known as 'compensating', as in Fig. 8.2(a) and (b), or 'uncompensating', as in Fig. 8.2(c). While the uncompensated version has only the zeroth ($\int_0^t g^*(t')dt'$) moment zero at the echo formation, the compensated version has both zeroth and first moments ($\int_0^t t'g^*(t')dt'$) zero, and so is insensitive to mean flow, but sensitive to acceleration or velocity fluctuations. At first sight, the uncompensated double PGSE NMR sequence would appear to have little value, but, as we shall see later, it can provide a valuable reference experiment.

The constraining of the $\mathbf{q}$ and $\mathbf{q}'$ vectors to be collinear, albeit with the same or opposite sense, is particularly useful in a wide class of double scattering experiments, especially where flow compensation is desired. However, as we will see in later sections, allowing $\mathbf{q}$ and $\mathbf{q}'$ to assume a range of relative orientations can result in some quite unique insights.

8.2 Double PGSE NMR and dispersion

8.2.1 Propagator and ensemble descriptions

For the moment, we focus our attention on the compensated double PGSE method. For simplicity, we will analyse the effect of this sequence under the assumption of the narrow gradient pulse approximation, although we may, by simulation or by use of the multiple propagator method, extend our analysis to account for finite pulse-width effects. Let us allow that at the first gradient pulse, the spin-bearing molecule is at position $\mathbf{r} = \mathbf{r}(0)$, while at application of the second pulse a time Δ later, its position is $\mathbf{r}' = \mathbf{r}(\Delta)$. After the 'mixing time' and at the application of the third gradient pulse it is $\mathbf{r}'' = \mathbf{r}(\Delta+\tau_m)$, and then at the final gradient pulse it is $\mathbf{r}''' = \mathbf{r}(2\Delta+\tau_m)$. The accumulated spin phase is therefore $\exp\left(i\mathbf{q}\cdot[\mathbf{r}(2\Delta+\tau_m) - \mathbf{r}(\Delta+\tau_m) - \mathbf{r}(\Delta) + \mathbf{r}(0)]\right)$. Thus the normalised echo signal may be written, as the ensemble average

$$E_D(\mathbf{q}) = \langle \exp\left(i\mathbf{q}\cdot[\mathbf{r}(2\Delta+\tau_m) - \mathbf{r}(\Delta+\tau_m) - \mathbf{r}(\Delta) + \mathbf{r}(0)]\right)\rangle \tag{8.1}$$

or, using using the conditional probabilities,

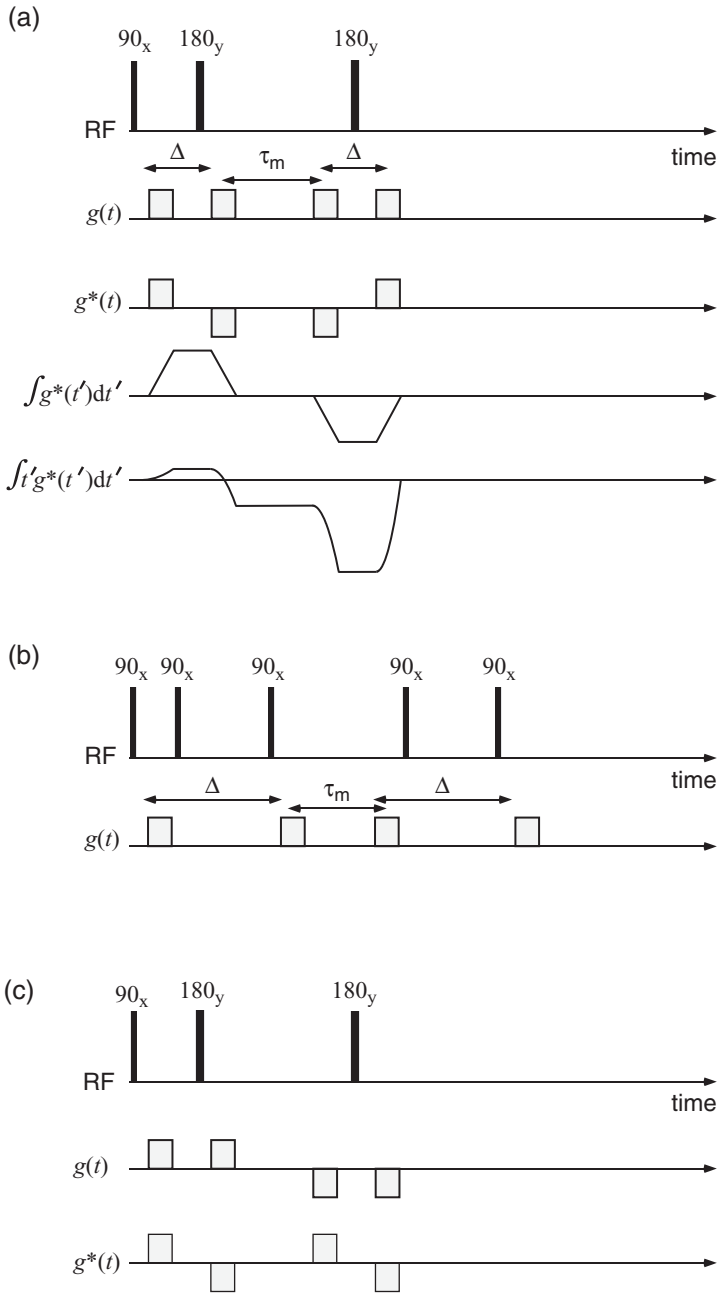

Fig. 8.2 Schematic double PGSE sequences in which the mixing time is indicated by τ_m. (a) Compensated double PGSE using spin echoes, (b) compensated double PGSE using stimulated echoes, (c) uncompensated double PGSE sequence.

$$E_D(\mathbf{q}) = \int d\mathbf{r}\rho(\mathbf{r}) \int d\mathbf{r}' P(\mathbf{r}|\mathbf{r}', \Delta) \int d\mathbf{r}'' P(\mathbf{r}'|\mathbf{r}'', \tau_m) \times \int d\mathbf{r}''' P(\mathbf{r}''|\mathbf{r}''', \Delta) \exp\left(i\mathbf{q} \cdot [\mathbf{r}''' - \mathbf{r}'' - \mathbf{r}' + \mathbf{r}]\right) \tag{8.2}$$

The propagator description turns out to be especially helpful when we look at the effect of restricted diffusion in double PGSE NMR sections. For the moment, however, we will take a look at how the method may be used to study fluctuating flows.

8.2.2 Dispersion measurement and the low-q limit

Single PGSE measurement of dispersion

Fluid dispersion is most easily described in terms of the ensemble of Lagrangian velocities, $\mathbf{v}(t)$, in which the mean flow velocity is $\mathbf{V} = \langle \mathbf{v}(t) \rangle$, while the fluctuation about the mean is $\mathbf{u}(t)$. In relating this to the PGSE NMR experiment, it becomes natural to substitute the displacement $\mathbf{r}(\Delta) - \mathbf{r}(0)$ by $\int_0^\Delta \mathbf{v}(t)dt$. For a single PGSE NMR sequence,

$$E_S(\mathbf{q}) = \left\langle \exp\left(i\mathbf{q} \cdot \int_0^\Delta \mathbf{v}(t)dt\right) \right\rangle = \exp(i\mathbf{q} \cdot \mathbf{V}\Delta) \left\langle \exp\left(i\mathbf{q} \cdot \int_0^\Delta \mathbf{u}(t)dt\right) \right\rangle \tag{8.3}$$

whence

$$|E_S(\mathbf{q})| \approx 1 - \tfrac{1}{2}q^2 \int_0^\Delta \int_0^\Delta \langle \mathbf{u}(t)\mathbf{u}(t') \rangle dt dt' \tag{8.4}$$

Note that these relationships allow us to define an effective dispersion coefficient according to the second definition of Section 6.1, namely

$$D^*_{eff} = -\frac{1}{\Delta} \lim_{q \to 0} \frac{\partial^2}{\partial q^2} \ln |E_S(q)| \tag{8.5}$$

where $q = |\mathbf{q}|$ and the dispersion is measured for the velocity component of $\mathbf{u}(t)$ in the direction of $\mathbf{q}$ [1]. Such an effective dispersion coefficient is simply obtained in practice by finding the slope of $\ln |E_S(q)|$ *vs* q^2 in the low-q limit. A typical flow geometry might be that through a cylindrical porous medium in which axial symmetry prevails. In that case $\parallel$ and $\perp$ directions may be defined and

$$D^*_{\parallel,\perp} = \frac{1}{2\Delta} \int_0^\Delta \int_0^\Delta \langle u_{\parallel,\perp}(t) u_{\parallel,\perp}(t') \rangle dt dt' \tag{8.6}$$

Such PGSE NMR methods have been extensively used [1–4] to study dispersion in porous media.

Double PGSE measurement of dispersion

For the compensated double PGSE NMR sequence shown in Fig. 8.2(a) and (b) the mean flow term $\mathbf{V}$ is automatically cancelled [5, 6], as illustrated in Fig. 8.3, and

$$E_D(\mathbf{q}) = \left\langle \exp\left(i\mathbf{q} \cdot \int_0^{\Delta} \mathbf{u}(t)dt \right) \times \exp\left(-i\mathbf{q} \cdot \int_{\tau_m+\Delta}^{\tau_m+2\Delta} \mathbf{u}(t)dt \right) \right\rangle \tag{8.7}$$

Now, in the low-q limit

$$E_D(\mathbf{q}) \approx 1 - \tfrac{1}{2}q^2 \Bigg[\int_0^{\Delta}\int_0^{\Delta} \langle \mathbf{u}(t)\mathbf{u}(t')\rangle dtdt' - 2\int_0^{\Delta}\int_{\tau_m}^{\tau_m+\Delta} \langle \mathbf{u}(t)\mathbf{u}(t')\rangle dtdt' + \int_{\tau_m+\Delta}^{\tau_m+2\Delta}\int_{\tau_m+\Delta}^{\tau_m+2\Delta} \langle \mathbf{u}(t)\mathbf{u}(t')\rangle dtdt' \Bigg] \tag{8.8}$$

and, allowing for the stationarity of $\mathbf{u}(t)$,

$$E_D(\mathbf{q}) \approx 1 - \tfrac{1}{2}q^2 \Bigg[2\int_0^{\Delta}\int_0^{\Delta} \langle \mathbf{u}(t)\mathbf{u}(t')\rangle dtdt' - 2\int_0^{\Delta}\int_{\tau_m}^{\tau_m+\Delta} \langle \mathbf{u}(t)\mathbf{u}(t')\rangle dtdt' \Bigg] \tag{8.9}$$

Equation 8.9 is particularly interesting. First, consider the case where the mixing time τ_m is much longer than any characteristic correlation time τ_v for the fluctuating $\mathbf{u}(t)$. Then the displacements during the two successive encoding intervals are completely uncorrelated and the second integral in the sum is zero. In that case the double PGSE NMR experiment will yield twice the stochastic part of the exponent for single PGSE NMR, and $E_D = |E_S|^2$. In this sense, any use of the low-q limit to define an effective dispersion coefficient using the double PGSE method, whatever the value of τ_m, implies an additional factor of two in our analysis of the initial slope.

Second, because there are two pairs of gradient pulses, each fulfilling the echo condition, the double PGSE sequence may be run with different directions for the first and second pulse pairs. Let us label these α and β. In that case we would rewrite eqn 8.8 as

$$E_D(q_\alpha, q_\beta) \approx 1 - \tfrac{1}{2} \Bigg[q_\alpha^2 \int_0^{\Delta}\int_0^{\Delta} \langle u_\alpha(t)u_\alpha(t')\rangle dtdt' + q_\beta^2 \int_{\tau_m+\Delta}^{\tau_m+2\Delta}\int_{\tau_m+\Delta}^{\tau_m+2\Delta} \langle u_\beta(t)u_\beta(t')\rangle dtdt' - 2q_\alpha q_\beta \int_0^{\Delta}\int_{\tau_m}^{\tau_m+\Delta} \langle u_\alpha(t)u_\beta(t')\rangle dtdt' \Bigg] \tag{8.10}$$

and by this means it is possible to correlate independent velocity directions at different times.

Measuring the velocity autocorrelation function

Finally, suppose we are able to make Δ sufficiently short ($\Delta \ll \tau_v$) that the fluctuating part of the velocity is effectively constant over the encoding interval Δ. In that case eqns 8.9 and 8.10 tell us that the double PGSE NMR method gives us a nice means of measuring the velocity autocorrelation function of $\mathbf{u}(t)$.

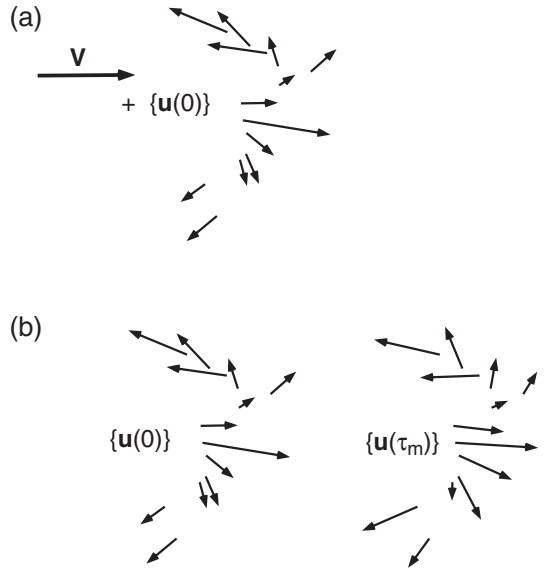

Fig. 8.3 The sensitivity of single and double PGSE to velocity distributions in the case $\Delta \ll \tau_v$. (a) Single PGSE, where the mean flow $\mathbf{V}$ imparts a phase shift $\exp(i\mathbf{q}\cdot\mathbf{V}\Delta)$ and the remaining velocity distribution contributes a phase factor $\langle\exp(i\mathbf{q}\cdot\mathbf{u}\Delta)\rangle$. (b) Double PGSE, where the mean flow term disappears and the phase factor arises from contributions at times 0 and τ_m as $\langle\exp(i\mathbf{q}\cdot[\mathbf{u}(0)-\mathbf{u}(\tau_m)]\Delta)\rangle$.

For $\Delta \ll \tau_v$, as $q^2 \to 0$, and with $\mathbf{q}$ in the α direction, we have

$$E_D(q_\alpha) \approx 1 - \tfrac{1}{2}q_\alpha^2\Big[2\Delta^2\langle u_\alpha^2\rangle dtdt' - 2\Delta^2\langle u_\alpha(0)u_\alpha(\tau_m)\rangle dtdt'\Big] \tag{8.11}$$

Clearly, analysis of the low-q^2 slope gives

$$-\frac{1}{\Delta}\lim_{q_\alpha\to 0}\frac{\partial^2}{\partial q_\alpha^2}\ln|E_D(q_\alpha)| = \langle u_\alpha^2\rangle\Delta - \langle u_\alpha(0)u_\alpha(\tau_m)\rangle\Delta \tag{8.12}$$

where $\langle\mathbf{u}(0)\mathbf{u}(\tau_m)\rangle$ is the velocity autocorrelation function, VACF. This function may be obtained by measuring the effective dispersion coefficient for the double PGSE NMR experiment as a function of τ_m, so that the normalised VACF is

$$\frac{\langle u_\alpha(0)u_\alpha(\tau_m)\rangle}{\langle u_\alpha^2\rangle} = \frac{D_{eff}(\infty) - D_{eff}(\tau_m)}{D_{eff}(\infty)} \tag{8.13}$$

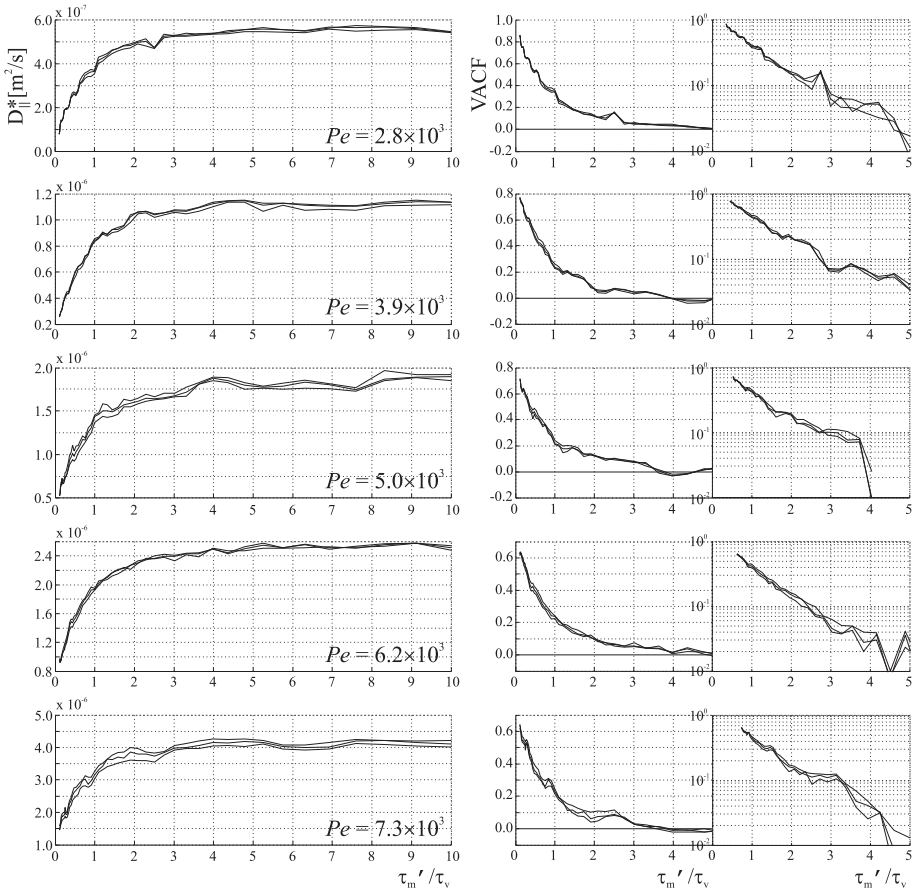

Fig. 8.4 τ_m dependence of apparent longitudinal dispersion for double PGSE and velocity autocorrelation functions (VACF) as a function of Péclet number. Note that the effective mixing time, $\tau'_m = \tau_m + \Delta$, is used. The semi-logarithmic plots of VACF reveal near single exponential behaviour. Note that the three curves in each graph were obtained by analysing the echo signals to three different levels of attenuation, exp(-0.3), exp(-0.4), and exp(-0.5). (Reproduced with permission from reference [7].)

Figure 8.4 shows the result of just such an experiment, performed for water flowing through a bead pack comprising 0.5 mm diameter latex spheres, and for a number of flow rates corresponding to Péclet numbers ranging from 2800 to 7300. In each case the times are shown normalised to the calculated flow correlation time $\tau_v = d/V$. The VACFs obtained appear single exponential and in each case exhibit a time constant close to τ_v

The extension to the case of a pair of gradient pulses of different direction is possible, given eqn 8.10. Here $\langle u_\alpha(0)u_\beta(\tau_m)\rangle$ may be obtained by from the 2-D function $E_D(q_\alpha, q_\beta)$, using the derivative $\partial^2/\partial q_\alpha \partial q_\beta$.

8.2.3 Reversible and irreversible dispersion

The double PGSE NMR experiment is particularly useful when it comes to distinguishing ensemble mean and temporal mean behaviour. For example, the steady velocity shear produced by a plane Couette cell has zero ensemble velocity average, despite there being a steady flow for each streamline. Of course, Taylor dispersion [8] will introduce fluctuations given sufficient time for molecules to laterally diffuse, but for the moment, let us assume that the 'static' distribution of velocities fluctuates much more slowly that the NMR timescale. The point is that the single PGSE NMR experiment will return a dispersion effect from this static component while the double PGSE NMR experiment will not.

Static and fluctuating parts

Suppose we represent these ideas mathematically by decomposing $\mathbf{u}(t)$ into a 'static' distribution $\delta\mathbf{u}$, with zero ensemble average, and a fluctuating component with zero time and ensemble average, $\mathbf{u}_f(t)$. In our double PGSE NMR experiment, the phase shifts arising from $\delta\mathbf{u}$ will be reversed in the second encoding and so any net contribution will be absent. Assuming that $\delta\mathbf{u}$ and $\mathbf{u}_f(t)$ are completely uncorrelated

$$D^*_{\text{single}} = \frac{1}{2}\langle \delta u^2\rangle \Delta + \frac{1}{2\Delta}\int_0^\Delta \int_0^\Delta \langle u_f(t)u_f(t')\rangle dt dt' \tag{8.14}$$

and

$$\begin{aligned} D^*_{\text{double}} = {} & \frac{1}{2\Delta}\int_0^\Delta \int_0^\Delta \langle u_f(t)u_f(t')\rangle dt dt' \\ & - \frac{1}{2\Delta}\int_0^\Delta \int_{\tau_m}^{\tau_m+\Delta} \langle u_f(t)u_f(t')\rangle dt dt' \end{aligned} \tag{8.15}$$

Following reference [7], D^*_{single} and D^*_{double} can be evaluated in the case where $u_f(t)$ is describable by an Ornstein–Uhlenbeck process, such that the autocorrelation function for $u_f(t)$ is given by the exponential decay

$$\langle u(t)u(0)\rangle = \langle u^2\rangle \exp(-t/\tau_c) \tag{8.16}$$

Allowing for the stationarity of the ensemble, the integrals are simple to perform and yield

$$D^*_{\text{single}} = \frac{1}{2}\langle \delta u^2\rangle \Delta + \langle u_f^2\rangle \tau_c \left[1 + \frac{\tau_c}{\Delta}\left(e^{-\frac{\Delta}{\tau_c}} - 1\right)\right] \tag{8.17}$$

and

$$\begin{aligned} D^*_{\text{double}} = {} & \langle u_f^2\rangle \tau_c \left[1 + \frac{\tau_c}{\Delta}\left(e^{-\frac{\Delta}{\tau_c}} - 1\right)\right] \\ & -\frac{1}{2}\langle u^2\rangle \tau_c \frac{\tau_c}{\Delta} \exp\left(-\frac{\tau_m}{\tau_c}\right)\left[1 - e^{-\frac{\Delta}{\tau_c}}\right]\left[e^{\frac{\Delta}{\tau_c}} - 1\right] \end{aligned} \tag{8.18}$$

Limiting cases

The various limiting cases resulting from eqn 8.18 are outlined in detail in reference [7]. Again, considering the limit where the velocity-encoding time, Δ, is much less than the fluctuation correlation time, τ_c.

$$D^*_{\text{single}} \approx \frac{1}{2}\langle \delta u^2 \rangle \Delta + \frac{1}{2}\langle u_f^2 \rangle \Delta \tag{8.19}$$

and

$$D^*_{\text{double}} \approx \frac{1}{2}\langle u_f^2 \rangle \Delta \left[1 - \exp\left(-\frac{\tau_m}{\tau_c} \right) \right] \tag{8.20}$$

Hence comparison of the single and double PGSE NMR experiments not only has the ability to reveal very slowly fluctuating or 'static' velocity spreads, it also provides a nice means by which temporal fluctuations may be accurately determined. As we will see in later sections, the double PGSE experiment has the capacity to significantly enhance the information content obtainable from the sole use of a single pair of gradient pulses.

It is worth noting that the double PGSE experiment, with its sequential reversal in the sign of velocity encoding, is not quite the same as a flow reversal experiment in which the apparent displacements are measured after an equal period of reversed flow. The distinction between these two types of measurement goes to the heart of the meaning of 'irreversibility' in complex flows, and distinctions which arise from the relevant length and timescales of each experiment.

8.3 Phase cycling for double PGSE NMR

Implementing double PGSE NMR is no trivial matter. It is customary to use spin-echo or stimulated-echo methods, so as to refocus unwanted background field inhomogeneity or protect the spins from T_2 relaxation. The extra RF pulses resulting from the doubling process can lead to complications. First, it is necessary to ensure that the phases chosen for the RF pulses do indeed produce the phase superposition required, for example as compensated or uncompensated PGSE versions. Indeed, where stimulated echoes are used, superpositions beyond these two simple cases are possible. Second, phase cycling to remove signal artifacts is inherently longer, since with every RF pulse added to a sequence comes the potential to introduce additional unwanted signal. The reason for this is that NMR pulse sequences are generally based on a presumption of perfect 90° or 180° RF pulses, which have the effect of manipulating the magnetisation generated by the first RF pulse in the train, but which themselves do not introduce additional coherence. Of course, in practice, these pulses are never perfect, if for no other reason than that the RF field is never perfectly homogeneous over the entire sample. For this reason, it is customary to phase-alternate these pulses, at the same time maintaining constant receiver phase locked to the first 90° excitation pulse, so as to always keep the desired signal positive whilst unwanted signals are cancelled. Each additional pulse means a doubling of the phase cycle, and so multiple RF pulse schemes necessarily involve much longer cycles.

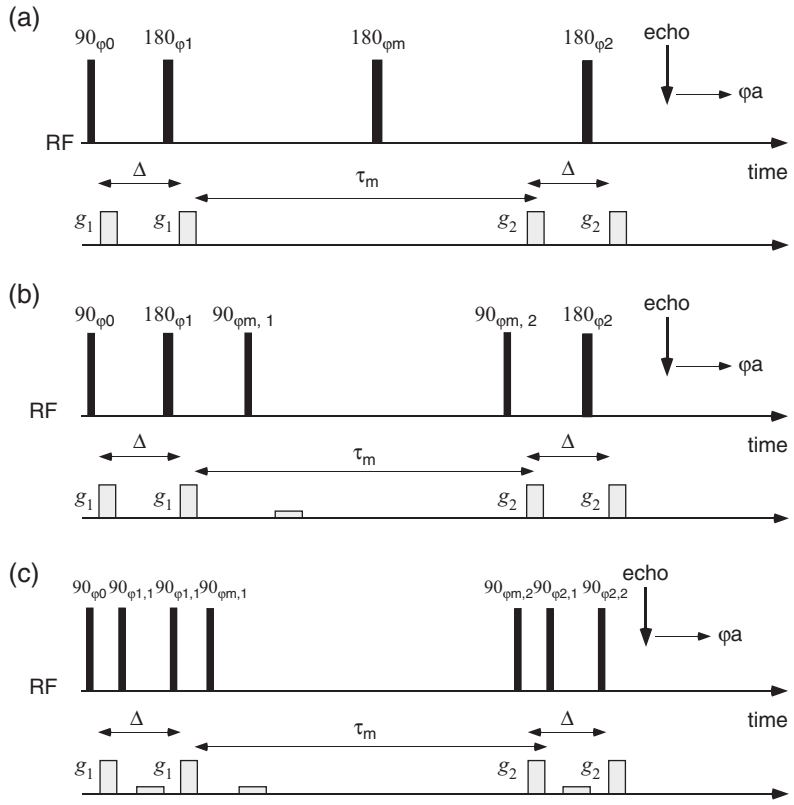

Fig. 8.5 Schematic RF and gradient pulse sequences for double PGSE NMR experiments in which the gradient pulse area ($g\delta$) is stepped. (a) $90^\circ - g_1 - 180^\circ - g_1 - \tau_m/2 - 180^\circ - \tau_m/2 - g_2 - 180^\circ - g_2 - acq$ version is shown. $g_1 = \pm g_2$ depending on whether compensated or uncompensated phase addition is required. The corresponding phase cycle is given in Table 8.1. (b) As for (a), but for the $90^\circ - g_1 - 180^\circ - g_1 - 90^\circ - \tau_m - 90^\circ - g_2 - 180^\circ - g_2 - acq$ version in which z-storage is used for the mixing period. The corresponding phase cycle is given in Table 8.2. (c) as for (a), but for the $90^\circ - g_1 - 90^\circ - 90^\circ - g_1 - 90^\circ - \tau_m - 90^\circ - g_2 - 90^\circ - 90^\circ - g_2 - acq$ version, in which z-storage is used for the encoding and mixing periods. The corresponding phase cycle is given in Table 8.3. Note that homospoil gradient pulses are included where stimulated echoes or z-storage are used. (Adapted from reference [9].)

8.3.1 Characterising the coherences

Let us deal first with the issue of wanted or unwanted coherence, a subject examined in detail in reference [9]. To do so we will take the pulse sequences of Fig. 8.5 as practical contenders for double PGSE NMR. In Fig. 8.5 a spin-echo scheme is shown, in which the mixing time also contains a 180° RF pulse so as to remove local field inhomogeneity dephasing. It is immediately obvious that this sequence is uncompensated, unless g_1

Table 8.1 Phase cycle table for double PGSE NMR based on three 180° refocusing pulses (Fig. 8.5(a)). Other combinations of RF pulse phases are possible but they generate no coherences beyond the two examples given.

$$90^\circ_{\varphi_0} - g_1 - 180^\circ_{\varphi_1} - g_1 - 180^\circ_{\varphi_m} - g_2 - 180^\circ_{\varphi_2} - g_2 - acq_{\varphi_a}$$

RF pulses				$g_1 = g_2$				$g_1 = -g_2$			
φ_0	φ_1	φ_m	φ_2	U	C	M	φ_a	U	C	M	φ_a
x	$\pm x$	$\pm x$	$\pm x$	$-$	0	0	x	0	$-$	0	x
x	$\pm y$	$\pm y$	$\pm y$	$+$	0	0	x	0	$+$	0	x

and g_2 are of opposite sign. Figures 8.5(b) and (c) show combinations where z-storage and stimulated echoes are used. In each case the RF pulse phase is labelled by a subscript φ, which may be taken to be x or y in the rotating frame, the first sequence in the train being taken to be always x, thus inducing a magnetisation along the y-axis of the rotating frame, which as discussed in Section 5.8, we take for convenience as the real axis of our transverse Argand plane. As discussed in Section 5.8 the effect of the very first gradient pulse is to induce a phase factor $\exp(i\phi_{1,1})$ and, using the rules outlined in that section, we must work out the cumulative effect of the subsequent RF and gradient pulses. In the case of the two pairs of gradient pulses labelled g_1 and g_2, the respective phases induced on a spin isochromat by each of the pulses are $\phi_{1,1}$, $\phi_{1,2}$, $\phi_{2,1}$, and $\phi_{2,2}$, with pair phase differences $\Delta\phi_1 = \phi_{1,2} - \phi_{1,1}$ and $\Delta\phi_2 = \phi_{2,2} - \phi_{2,1}$. The desired phase factor for the compensated (C) double PGSE sequence is $\exp(i\Delta\phi_1 - i\Delta\phi_2)$, while that of the uncompensated (U) is $\exp(i\Delta\phi_1 + i\Delta\phi_2)$.

8.3.2 Coherence selection

The pulse trains of Fig. 8.5 may be analysed through a process that is tedious [9], but with outcomes as summarised in the tables. Note that in the case of the all 180° pulse sequence of Fig. 8.5(a), both pure uncompensated and compensated signals can be obtained, the latter requiring opposite-signed g_1 and g_2 pulse pairs. By contrast, the pulse sequence comprising two spin echoes with a period of z-storage for the mixing period will always result in a superposition of uncompensated (U) and compensated (C) signals. The reason for this is straightforward: since the effect of the first gradient pulse pair is an induced phase difference $\exp(i\Delta\phi_1) = \exp(i[\phi_{1,1} - \phi_{1,2}])$. z-storage involves the maintenance of only one component of the magnetisation generated in the transverse Argand plane, the other component remaining in that place during the mixing time being destroyed by homospoiling or T_2 relaxation. In algebraic terms, we retain only the $\cos(\Delta\phi_1)$ or $\sin(\Delta\phi_1)$ from $\exp(i\Delta\phi_1)$. The result is that both positive and negative phase differences are present to be acted upon by the second gradient pulse pair in the second spin echo. Thus we will find both $\Delta\phi_1 + \Delta\phi_2$ and $-\Delta\phi_1 + \Delta\phi_2$ in the final signal contributions. To obtain pure U or C, a phase cycle involving both x- and y-phase storage pulses is needed. By this means, the appropriate admixture of real and imaginary terms can be obtained after the recall RF pulse following z-storage.

Table 8.2 Phase cycle table for double PGSE NMR based on two 180° refocusing pulses and one 90° pair for z-storage during the mixing time (Fig. 8.5(b)). Again, 180° pulses may have phases of either sign, for the same effect. In this table we include the y phase only for convenience. The table is not exhaustive but gives a sample of outcomes, all of which contain a superposition of U and C terms.

$$90^\circ_{\varphi_0} - g_1 - 180^\circ_{\varphi_1} - g_1 - 90^\circ_{\varphi_{m,1}} - 90^\circ_{\varphi_{m,2}} - g_2 - 180^\circ_{\varphi_2} - g_2 - acq_{\varphi_a}$$

RF pulses				$g_1 = g_2$				$g_1 = -g_2$			
φ_0	φ_1	$\varphi_{m,1}$ $\varphi_{m,2}$	φ_2	U	C	M	φ_a	U	C	M	φ_a
x	$\pm y$	$(-x, x)$	$\pm y$	$+$	$+$	0	x	$+$	$+$	0	x
x	$\pm y$	(x, x)	$\pm y$	$-$	$-$	0	x	$-$	$-$	0	x
x	$\pm y$	$(-y, y)$	$\pm y$	$+$	$-$	0	x	$-$	$+$	0	x
x	$\pm y$	(y, y)	$\pm y$	$-$	$+$	0	x	$+$	$-$	0	x
x	$\pm y$	$(-y, y)$	$\pm y$	$+$	$+$	0	y	$+$	$+$	0	y
x	$\pm y$	(y, y)	$\pm y$	$-$	$-$	0	y	$-$	$-$	0	y

Table 8.3 Phase cycle table for double PGSE NMR based on two stimulated echoes and one 90° pair for z-storage during the mixing time (Fig. 8.5(c)). The table is not exhaustive but gives a sample of outcomes. Note that the mixing term, labelled M, is generally undesired and can be removed by a suitable phase cycle superposition.

$$90^\circ_{\varphi_0} - g_1 - 90^\circ_{\varphi_{1,1}} - 90^\circ_{\varphi_{1,2}} - g_1 - 90^\circ_{\varphi_{m,1}} - 90^\circ_{\varphi_{m,2}} - g_2 - 90^\circ_{\varphi_{2,1}} - 90^\circ_{\varphi_{2,2}} - g_2 - acq_{\varphi_a}$$

RF pulses				$g_1 = g_2$				$g_1 = -g_2$			
φ_0	φ_1	$\varphi_{m,1}$ $\varphi_{m,2}$	φ_2	U	C	M	φ_a	U	C	M	φ_a
x	(x, x)	(x, x)	(x, x)	$-$	$-$	$-$	x	$-$	$-$	$-$	x
x	(y, y)	(y, y)	(y, y)	$+$	$-$	$+$	y	$-$	$+$	$-$	y
x	(x, x)	(x, x)	(x, x)	$+$	$-$	$+$	y	$-$	$+$	$-$	y
x	(y, y)	(x, x)	(y, y)	$-$	$-$	$-$	x	$-$	$-$	$-$	x
x	(x, x)	(x, x)	(y, y)	$+$	$+$	$-$	y	$+$	$+$	$-$	y
x	(y, y)	(x, x)	(x, x)	$+$	$+$	$-$	y	$+$	$+$	$-$	y
x	(y, y)	(y, y)	(x, x)	$-$	$+$	$+$	x	$+$	$-$	$-$	x
x	(x, x)	(y, y)	(y, y)	$-$	$+$	$+$	x	$+$	$-$	$-$	x

The most convenient form of the double PGSE NMR sequence, where spins are to be protected from T_2 relaxation, is that involving two stimulated echoes and one z-storage period, as shown in Fig. 8.5(c). Intriguingly, this sequence generates yet another coherence, neither U nor C in character. Instead it is of the form $\exp(i[\phi_{1,1} + \phi_{1,2}] - i[\phi_{2,1} + \phi_{2,2}])$ and denoted M. Where the magnitudes of g_1 and g_2 are the same, as would customarily be the case, this phase factor approximately represents an encoding for displacement over the mixing time τ_m. It is an unintended and undesired contribution and requires suitable phase cycling to be removed.

Table 8.4 32-step phase cycle table for the double PGSE NMR sequence used to measure the non-local dispersion tensor, and based on two 180° refocusing pulses and one 90° pair for z-storage during the mixing time τ. (Fig. 8.6(b) and (c)). The eight steps shown are repeated for positive and negative first 180° RF pulse phases so as to remove FID effects from this pulse, and repeated a second time, with opposite sign excitation pulse phase and opposite sign acquisition phase, to remove baseline artifacts.

φ_0	φ_1	$\varphi_{m,1}$ $\varphi_{m,2}$	φ_2	φ_a
x	$\pm y$	(x,x)	y	x
x	$\pm y$	$(-x,-x)$	$-y$	x
x	$\pm y$	(y,y)	$-x$	$-x$
x	$\pm y$	$(-y,-y)$	x	$-x$
x	$\pm y$	$(x,-x)$	y	$-x$
x	$\pm y$	$(-x,x)$	$-y$	$-x$
x	$\pm y$	$(y,-y)$	$-x$	x
x	$\pm y$	$(-y,y)$	x	x

Table 8.3 exhibits a wide range of U, C, and M superpositions. By suitable combinations each coherence may be selected as desired. For example, to obtain a pure compensated double PGSE outcome using the stimulated echo, the z-storage sequence of Fig. 8.5(c), the $(x,x)(x,x)(x,x) - x$ and $(y,y)(y,y)(y,y) - y$ combinations serve to eliminate U and M. Where $g_1 = g_2$ the summed cycle is effective, whereas for $g_1 = -g_2$ the difference may be used.

8.4 Non-local dispersion tensor

In Chapter 2, the non-local dispersion tensor was introduced. Defined by the relation

$$\underline{\underline{D}}^{NL}(\mathbf{R},\tau) = \int P(\mathbf{r})\mathbf{u}_{\mathbf{E}}(\mathbf{r},0)P(\mathbf{r}|\mathbf{r}+\mathbf{R},\tau)\mathbf{u}_{\mathbf{E}}(\mathbf{r}+\mathbf{R},\tau)d\mathbf{r} \tag{8.21}$$

$\underline{\underline{D}}^{NL}$ provides insight regarding spatio-temporal correlations in the fluctuating part of the velocity field in dispersive flow. Its measurement provides one of the more technically challenging applications of double PGSE NMR methods [10], requiring the use of a superposition of signals arising from a pulse sequences such as those shown in Fig. 8.6. The elements of the $\underline{\underline{D}}^{NL}$ tensor can be extracted from the response of the spin-echo signal superposition to the independent dimensions of the various gradient pulses, an analysis that requires a careful signal fitting in the low-q domain.

8.4.1 The pulse sequence for velocity and displacement encoding

The pulse sequences of Fig. 8.6 have the gradients $\mathbf{g}$ and $\mathbf{g}_u$ stepped independently [11], where $\mathbf{q}_D = \gamma\mathbf{g}\delta_D$ and $\mathbf{q}_u = \gamma\delta_u\Delta_u\mathbf{g}_u$ are, respectively, conjugate to the dynamic displacement, $\mathbf{R}$, and the local velocity, $\mathbf{v}$. As shown in Figs 8.6(b) and (c), the displacement gradient pulse may be split in two around a 180° RF pulse, thus enabling background inhomogeneity refocusing [12]. Hence $\delta_u = \delta$ and $\delta_D = 2\delta$.

In the case of $\mathbf{q}_D$, it is helpful to use a fully bi-polar displacement encoding to produce a good representation, via Fourier transformation, of propagator information

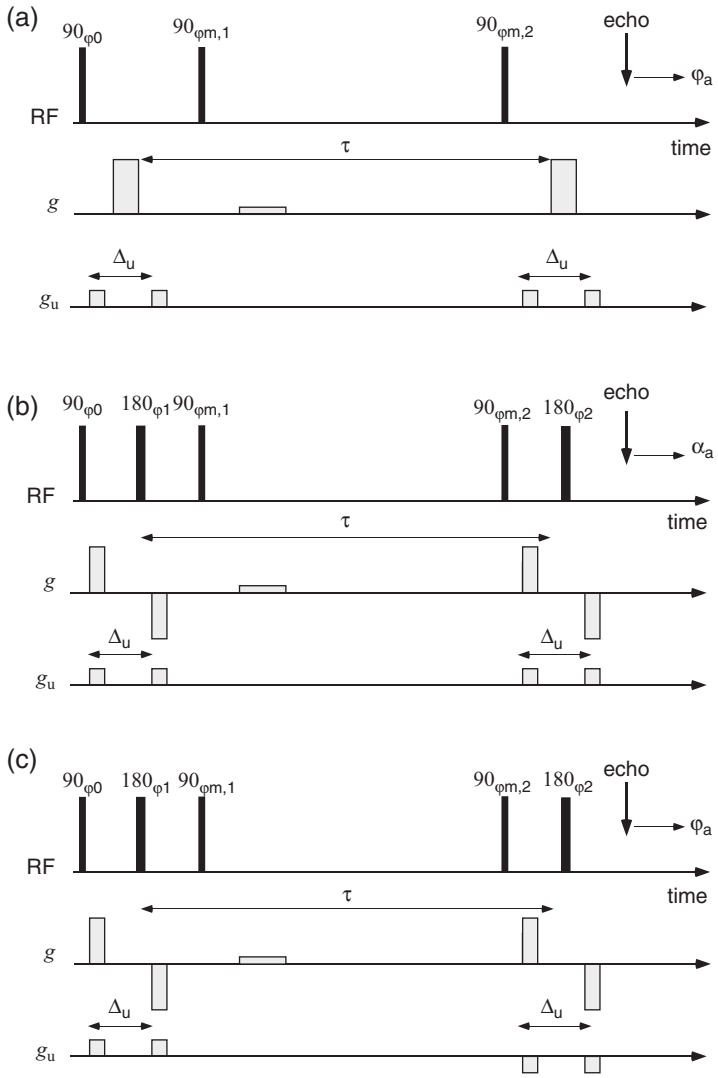

Fig. 8.6 (a) Schematic RF and gradient pulse sequences for non-local dispersion measurement, in which the gradient pulses labelled g refer to displacement encoding, and those labelled g_u are for compensated or uncompensated velocity encoding depending on the sign of the second g_u pair. τ is the mixing time over which displacement is measured. (b) Practical implementation of the compensated sequence based on splitting of the displacement gradient pulse into two, around a 180° RF pulse for background inhomogeneity refocusing. The phase cycle is shown in Table 8.4. (c) As for (b), but for the uncompensated sequence. (Adapted from Hunter *et al.* [11].)

in the space $\mathbf{R}$ of $\underline{\underline{D}}^{NL}(\mathbf{R},\tau)$. For the velocity encoding, the low-q_u limit is used, as in the case of direct measurements of the velocity autocorrelation function via double PGSE experiments [7], described in Section 8.1.2. As in those measurements, the time τ, the separation of the double PGSE pulses, corresponds to a 'mixing-time' in the NMR sense, and is the temporal displacement referred to in $\underline{\underline{D}}^{NL}(\mathbf{R},\tau)$.

The NMR signal

The NMR signal is acquired at the final spin echo from the sequence shown in Fig. 8.6(b). When normalised it can be written

$$\begin{aligned} E(\mathbf{q}_D,\mathbf{q}_u) = \iint & \exp(i\mathbf{q}_D{\cdot}\mathbf{R}) \exp(-i\mathbf{q}_u \cdot (\mathbf{u}_E(\mathbf{r},0) + \langle\mathbf{v}\rangle)) \\ & \times P(\mathbf{r}) P(\mathbf{r}|\mathbf{r}+\mathbf{R},\tau) \exp(i\mathbf{q}_u{\cdot}(\mathbf{u}_E(\mathbf{r}+\mathbf{R},\tau) + \langle\mathbf{v}\rangle)) d\mathbf{R} d\mathbf{r} \end{aligned} \tag{8.22}$$

The next step in the analysis involves taking the inverse Fourier transform in the $\mathbf{q}_D$ dimension, thus taking us to the domain of the displacement $\mathbf{R}$ and the intermediate signal

$$\begin{aligned} S(\mathbf{R},\mathbf{q}_u) = \mathcal{F}^{-1}_{\mathbf{q}_D}\{E(\mathbf{q}_D,\mathbf{q}_u)\} = \int & \exp(-i\mathbf{q}_u{\cdot}\mathbf{u}_E(\mathbf{r},0)) P(\mathbf{r}) P(\mathbf{r}|\mathbf{r}+\mathbf{R},\tau) \\ & \times \exp(i\mathbf{q}_u{\cdot}\mathbf{u}_E(\mathbf{r}+\mathbf{R},\tau)) d\mathbf{r} \end{aligned} \tag{8.23}$$

This notation can be compacted through a convenient change [11] in which the E subscript is dropped, and the integral over starting positions rewritten as an ensemble average. Using this approach the integrand term $P(\mathbf{r})P(\mathbf{r}|\mathbf{r}+\mathbf{R},\tau)$ is replaced by the averaged propagator $\overline{P}(\mathbf{R},\tau)$. Hence

$$\begin{aligned} \underline{\underline{D}}^{NL}(\mathbf{R},\tau) &= \int P(\mathbf{r})\mathbf{u}_{\mathbf{E}}(\mathbf{r},0) P(\mathbf{r}|\mathbf{r}+\mathbf{R},\tau)\mathbf{u}_{\mathbf{E}}(\mathbf{r}+\mathbf{R},\tau) d\mathbf{r} \\ &= \big\langle \mathbf{u}(0)\overline{P}(\mathbf{R},\tau)\mathbf{u}(\tau)\big\rangle \end{aligned} \tag{8.24}$$

By this means, eqn 8.23 may be rewritten

$$S(\mathbf{R},\mathbf{q}_u) = \big\langle \exp(-i\mathbf{q}_u{\cdot}\mathbf{u}(0)\overline{P}(\mathbf{R},\tau) \exp(i\mathbf{q}_u{\cdot}\mathbf{u}(\tau)\big\rangle \tag{8.25}$$

Of course, it is important to treat this new notation as only a shorthand for the full integral expression.

The low-q limit and extracting the elements of D^{NL}

The elements of $\underline{\underline{D}}^{NL}$ can be found by carrying out a succession of measurements using different gradient directions. To illustrate how these elements are extracted, it is helpful to consider, as an example, the case where displacement ($\mathbf{q}_D$) encoding and velocity ($\mathbf{q}_u$) encoding are both in the Z direction. The next step in the analysis is to expand the echo-attenuation expression in the low-q_u limit. For the compensated sequence

$$\begin{aligned} S_{comp}(Z,q_u) = \big\langle & \big(1 - iq_u u_z(0) - \tfrac{1}{2}q_u^2 u_z(0)^2 + \ldots.\big)\, \overline{P}(Z,\tau) \\ & \times \big(1 + iq_u u_z(\tau) - \tfrac{1}{2}q_u^2 u_z(\tau)^2 - \ldots.\big)\big\rangle \end{aligned} \tag{8.26}$$

where q_u represents the magnitude of a $\mathbf{q}_u$ vector applied along the z-axis. The equivalent expansion for the compensated pulse sequence gives

$$\begin{aligned} S_{comp}(Z,q_u) = \Big\langle \Big(& 1 + iq_u\left(u_z(0) - u_z(\tau)\right) - \tfrac{1}{2}q_u^2\left(u_z(0)^2 + u_z(\tau)^2\right) \\ & + q_u^2 u_z(0)u_z(\tau)\Big)\overline{P}(Z,\tau)\Big\rangle \\ & + iO(q_u^3) + O(q_u^4) \end{aligned} \tag{8.27}$$

where truncation errors in q_u^3 and q_u^4 are notated separately, since they arise respectively from imaginary and real parts of the data.

Sequence superposition

The desired non-local dispersion tensor element is present as a partial coefficient of q_u^2. The trick therefore is to extract it cleanly. This involves the use of a second experiment performed with the sign of the second velocity-encoding pulse reversed, as shown Fig. 8.6(b). This version yields

$$\begin{aligned} S_{uncomp}(Z,q_u) &= \exp\left(i2q_u\left\langle v_z\right\rangle\right) \\ &= \times\Big\langle\Big(1 + iq_u\left(u_z(0) + u_z(\tau)\right) - \tfrac{1}{2}q_u^2\left(u_z(0)^2 + u_z(\tau)^2\right) \\ &\quad - q_u^2 u_z(0)u_z(\tau)\Big)\overline{P}(Z,\tau)\Big\rangle \\ &\quad + iO(q_u^3) + O(q_u^4) \end{aligned} \tag{8.28}$$

The extra phase factor, $\exp\left(i2q_u\left\langle v_z\right\rangle\right)$, at the beginning of the expression, arises because the uncompensated version of the double PGSE experiment is sensitive to the mean flow. The phase factor is easily determined and corrected by examining the data $E(0,q_u)$. Performing this phase correction and implementing a difference superposition results in

$$\begin{aligned} S_{comp}(Z,q_u) - \exp(-i2q_u\left\langle v_z\right\rangle)S_{uncomp}(Z,q_u) &= -i2q_u\left\langle u_z\overline{P}(Z,\tau)\right\rangle \\ &\quad + 2q_u^2\left\langle u_z(0)\overline{P}(Z,\tau)u_z(\tau)\right\rangle \\ &\quad + iO(q_u^3) + O(q_u^4) \end{aligned} \tag{8.29}$$

A fit of q_u^2 to the real part of the superposition represented by eqn 8.29 provides the desired encoding for the non-local dispersion tensor component $D_{zz}(Z,\tau)$. Alternatively, the tensor may be obtained from the superposition

$$\begin{aligned} S_{comp}(Z,q_u) - \exp(-i2q_u\left\langle v_z\right\rangle)S_{uncomp}(Z,q_u) & \\ + S_{comp}(Z,-q_u) - \exp(i2q_u\left\langle v_z\right\rangle)S_{uncomp}(Z,-q_u) & \\ = +4q_u^2\left\langle u_z(0)\overline{P}(Z,\tau)u_z(\tau)\right\rangle + O(q_u^4) & \end{aligned} \tag{8.30}$$

The complete D^{NL} tensor

The complete non-local tensor contains elements for each combination of velocity and displacement direction, and can be generalised using the dimension subscripts α and β for the initial and final velocity and $\mathbf{q}_u$, respectively, and γ, for the direction of the displacement encoding, denoted X_γ. The non-local dispersion tensor, written in this subscript form is

$$D^{NL}_{\alpha\beta}(X_\gamma, \tau) = \left\langle u_\alpha(0)\overline{P}(X_\gamma, \tau)u_\beta(\tau)\right\rangle \tag{8.31}$$

The three choices of direction available for the three different encodings give a total of 27 terms. However, it turns out that for axial flow in a porous medium there are six non-zero independent terms [11].

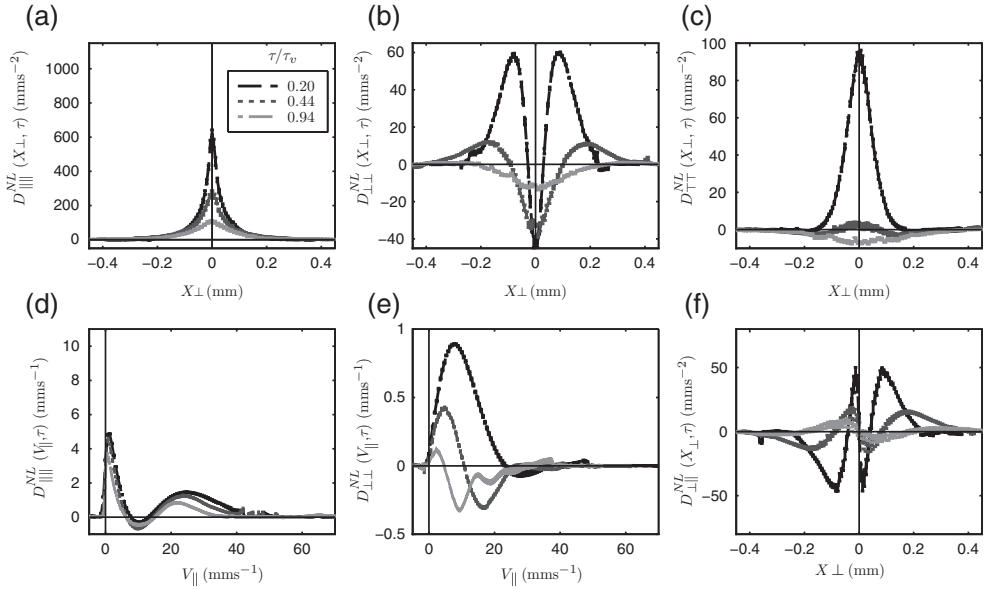

Fig. 8.7 The six independent non-local dispersion tensor components for flow in a random 0.5 mm diameter beadpack of porosity 0.38, measured for three different values of τ. The components in the direction of the main flow are plotted as average velocity, rather than displacement. The error bars show the estimate of the error in the fit to q^2. (Reproduced from Hunter *et al.* [11].)

Omitting the truncation errors, the general expression for the signal superposition of eqn 8.29 becomes

$$\begin{aligned}
&\exp(iq_{u\alpha}\langle v_\alpha\rangle - iq_{u\beta}\langle v_\beta\rangle)S_{comp}(X_\gamma, q_{u\alpha,\beta}) \\
&-\exp(iq_{u\alpha}\langle v_\alpha\rangle + iq_{u\beta}\langle v_\beta\rangle)S_{uncomp}(X_\gamma, q_{u\alpha,\beta})\} \\
&\qquad = iq_{u\alpha}\left\langle u_\alpha\overline{P}(X_\gamma,\tau)\right\rangle \\
&\qquad\quad + iq_{u\beta}\left\langle \overline{P}(X_\gamma,\tau)u_\gamma\right\rangle \\
&\qquad + 2q_{u\alpha}q_{u\beta} \\
&\qquad\quad \times\left\langle u_\alpha(0)\overline{P}(X_\gamma,\tau)u_\beta(\tau)\right\rangle
\end{aligned} \tag{8.32}$$

where $q_{u\alpha,\beta}$ means the first and second pairs of velocity-encoding gradients are along α and β, respectively. As before, the extraction of D^{NL} involves either fitting the real part to to $q_{u\alpha}q_{u\beta}$ or using a superposition of $S_{comp}(X_\gamma, -q_{u\alpha,\beta})$ and $S_{un}(X_\gamma, -q_{u\alpha,\beta})$.[1]

8.4.2 Non-local dispersion for porous media flow

Figure 8.7 shows the results obtained using the the double PGSE NMR sequences of Fig. 8.6(b) and (c) for distilled water flowing at a tube velocity of about 10 mm s^{-1} through a randomly distributed 500-micron diameter latex sphere bead pack ($\tau_v \approx$ 50 ms) of 10 mm tube diameter. The velocity-encoding time, $\Delta_u = 2$ ms, is much smaller than the displacement encoding times of 10, 21.5, and 46.3 ms. Each measurement takes around 8 h in a 400 MHz magnet. The directions α, β, and γ are fixed by the flow to be longitudinal ($\parallel$) or transverse ($\perp$).

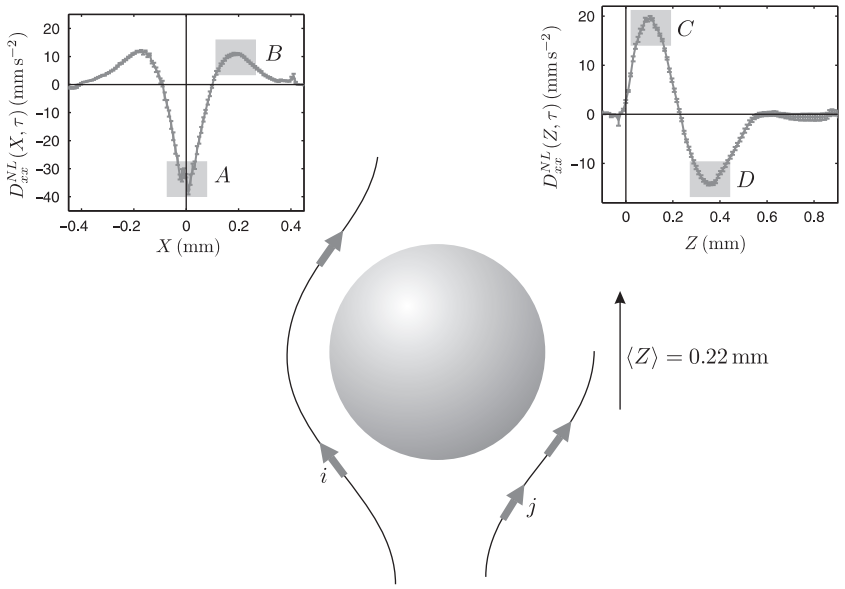

Fig. 8.8 Possible behaviour of particles moving around a bead with experimental measurements. Consider $D_{xx}^{NL}(X,\tau)$ and $D_{xx}^{NL}(Z,\tau)$ at an encoding time such that the mean displacement is approximately half a bead diameter. A guess is made that particles similar to i make up that parts of the graphs A and D, whereas the correlations shown as B and C are from particles similar to j. (Reproduced from Hunter *et al* [11].)

For each of the graphs shown in Fig. 8.7, integration over the displacement X_γ returns one data point for the velocity autocorrelation function at that time. Clearly there is extra information in the non-local dispersion tensor. Just to illustrate the sort of physical insight that is possible, it is instructive to focus attention on the two

[1]Where the velocity encoding is along a direction with bulk flow, no phase correction is necessary.

tensor components, $D_{xx}^{NL}(X,\tau)$ and $D_{xx}^{NL}(Z,\tau)$. When integrated over displacement, X or Z, both describe exactly the same temporal correlation function. But look at what they tell us once extracted, as shown in Fig. 8.8, for an encoding time such that the mean displacement is approximately half a bead diameter. They have oscillatory character, with positive lobes (correlations), negative lobes (anti-correlations), and decays to zero (de-correlation). An anti-correlation arises when flows have correlated magnitudes, but opposite directions, exactly as once might expect when considering the transverse velocity components for longitudinal flow in the vicinity of a bead, as seen in the streamline illustrated in the lower part of Fig. 8.8. These anti-correlations are clearly visible in $D_{xx}^{NL}(X,\tau)$ and $D_{xx}^{NL}(Z,\tau)$, at zero displacement along X for $D_{xx}^{NL}(X,\tau)$ and displaced along the flow for $D_{xx}^{NL}(Z,\tau)$. Correlations are visible for small displacements for both tensor elements, while at distances much greater than a bead diameter all correlation disappears.

8.4.3 Non-local dispersion for pipe flow

A nice example of the use of the non-local dispersion tensor to glean physical insight is the case of Taylor dispersion in pipe flow, where diffusion across streamlines causes molecules to be swept apart in the shear field of longitudinal flow. The flow field is shown in Fig. 8.9, and the relevant non-local dispersion is associated with transverse diffusive displacements across stream lines, for which the longitudinal total velocity field is $v_z = \bar{v}(1 - r^2/a^2)$, while the mean-referenced field is $u_z = \bar{v}(1 - 2r^2/a^2)$, $\bar{v}$ being the average longitudinal velocity in the pipe.

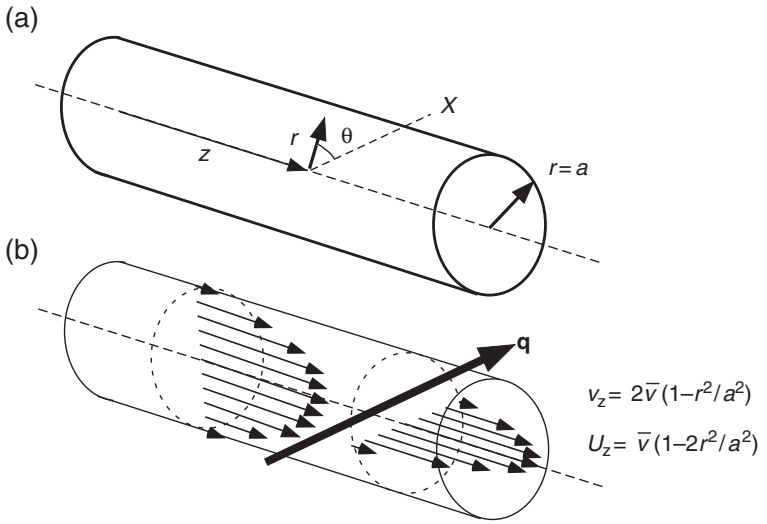

Fig. 8.9 Coordinates for laminar flow in a pipe. The relevant non-local dispersion is associated with transverse diffusive displacements across the stream lines, as probed by wavevector $\mathbf{q}$. The direction of $\mathbf{q}$ defines the displacement axis X used as a reference for cylindrical polar angle θ.

For the pipe, an easy route to D^{NL} is afforded by calculating the Fourier transform of the non-local dispersion tensor with respect to $\mathbf{q}$, the wavevector conjugate to X.

$$\begin{aligned}
E(\mathbf{q}) &= \iint d\mathbf{r}d\mathbf{r}' u_z(\mathbf{r},0)P(\mathbf{r})P(\mathbf{r}|\mathbf{r}',\tau)u_z((\mathbf{r}',t)\exp\left(-i\mathbf{q}\cdot(\mathbf{r}'-\mathbf{r}'\right)) \\
&= \frac{1}{\pi a^2}\sum_{n,k}\exp(-\beta_{nk}^2 D_0\tau/a^2)A_{nk}^2 \\
&\quad \times\int_0^{2\pi}\int_0^{2\pi}\int_0^a\int_0^a \bar{v}(1-2r^2/a^2)J_n(\beta_{nk}r/a)\cos(n\theta)J_n(\beta_{nk}r'/a)\cos(n\theta')\bar{v}(1-2r'^2/a^2) \\
&\quad \times\exp(iq(r\cos\theta - r'\cos\theta'))d\theta d\theta' dr dr' \\
&= \frac{1}{\pi a^2}\sum_{n,k}\exp(-\beta_{nk}^2 D_0\tau/a^2)A_{nk}^2 \\
&\quad |\int_0^{2\pi}\int_0^a\int_0^a \bar{v}(1-2r^2/a^2)J_n(\beta_{nk}r/a)\cos(n\theta)\exp(iq(r\cos\theta))d\theta dr|^2
\end{aligned} \tag{8.33}$$

where A_{nk} is given by eqns 7.33 and 7.34, and β_{nk} are the roots of eqn 7.35. Labelling the integral inside the modulus signs I_1, and noting the identity $J_n(x) = (i^{-n}/2\pi)\int_0^{2\pi}\exp(ix\cos\theta)\exp(in\theta)d\theta$,

$$\begin{aligned}
I_1 &= \int_0^a\int_0^a \bar{v}(1-2r^2/a^2)J_n(\beta_{nk}r/a)\left[\frac{2\pi}{i^n}\frac{1}{2}J_n(qr) + \frac{2\pi i^{4n}}{i^n}\frac{1}{2}J_n(qr)\right]rdr \\
&= \frac{2\pi}{i^n}\int_0^a \bar{v}(1-2r^2/a^2)J_n(\beta_{nk}r/a)J_n(qr)rdr
\end{aligned} \tag{8.34}$$

I_1 may be easily obtained by numerical integration, with eqn 8.33 Fourier transformed to give the non-local dispersion tensor element $D_{zz}^{NL}(X,\tau)$. The results, for a range of values of non-dimensionalised τ values, are shown in Fig. 8.10. Also shown is the integral with respect to X of each of the $D_{zz}^{NL}(X,\tau)$ curves, plotted as a function of τ. This, of course, is the velocity autocorrelation function, which decays, in accordance with Taylor–Aris theory [8, 13, 14], as $\exp(-D_0\mu_1^2\tau/a^2)$, where $\mu_1 = 3.83$ is the first root of the zeroth order Bessel function.[2]

The physical interpretation of the positive and negative correlation and anti-correlation lobes of Fig. 8.10 follows naturally from our knowledge of the Poiseuille flow field. Most obviously, the positive correlation lobe at $X = 0$ decays with time, as more diffusion occurs, and the return to origin probability drops. The negative lobes near $X = \pm a$ arise because of the dominant role of those molecules, the velocities of which change in sign of u_z when displacing by a, the pipe radius. At short τ, these negative lobes are unpopulated, growing as the diffusion time increases and molecules have the opportunity to make significant transverse migrations. The last

[2]The decay is, in fact, multiexponential, but the μ_1 term is dominant.

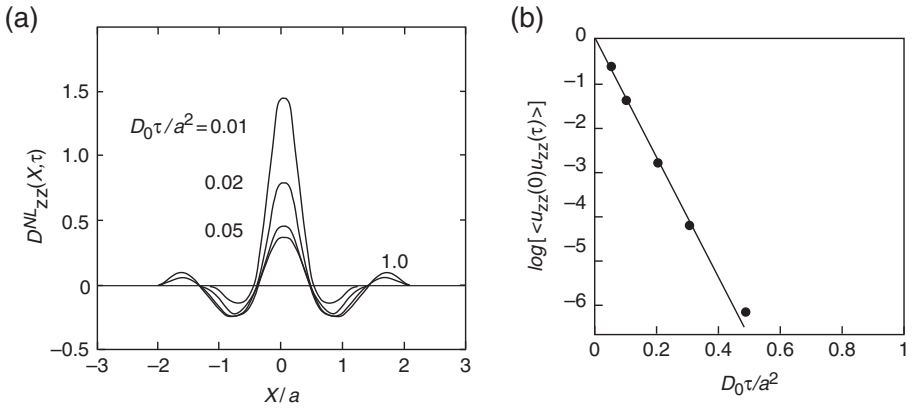

Fig. 8.10 (a) Non-local dispersion tensor element $D_{zz}^{NL}(X,\tau)$ for pipe flow at times τ such that $D_0\tau/a^2$ takes values of 0.01,0.02, 0.05, and 1. (b) Normalised velocity autocorrelation function $\langle u_z(0)u_z(\tau\rangle$ obtained by integrating the curves in (a). The slope of the line is 3.83^2.

lobes to appear are those positive lobes at displacements near $X = \pm 2a$. These are a direct consequence of the symmetry of the velocity field. Once $D_0\tau/a^2 \gtrsim 1$, the lobe structure persists, since for long τ values all transverse displacements are explored and an asymptotic $D_{zz}^{NL}(X,\tau)$ is reached because of unique starting and end-point velocities for displacements right across the pipe diameter, irrespective of the time taken to make the traverse. Of course, the integral across X of this asymptotic limit is zero, as is immediately apparent in the VACF values shown in Fig. 8.10.

8.5 Restricted diffusion and double wavevector encoding with long mixing time

In studies of fluid advection and dispersion, the advantages of double PGSE NMR are obvious, given the capacity of this method to remove phase shifts due to mean flow. But it also happens that double wavevector encoding provides new insights even when molecular transport is governed by Brownian motion alone and, in particular, when that Brownian motion is restricted by molecular collision with boundaries. A first suggestion of this use was by Cory, Garroway, and Miller [15], who proposed that double encoding could be used to examine effects of local compartment anisotropy in porous media. The first detailed theoretical study of the implications of double wavevector encoding for molecules diffusing in a porous medium was due to P.P. Mitra, who, in a remarkable paper in 1995, showed that where restricted diffusion occurs, even if the pore geometry is isotropic, the echo attenuation paradoxically depends on the relative directions in which the two pairs of gradient pulses are applied. We will examine this paradox in more detail in Section 8.6.

8.5.1 Correlated and uncorrelated phase encoding

One of the remarkable features of NMR is that phase-sensitive signals are acquired from an ensemble of nuclear spins in a coherent manner. In particular, the phase for

each spin may undergo a number of controlled evolutions before the signal is measured. In the case of double wavevector encoding, we deal specifically with independent evolution periods associated with each wavevector gradient pulse pair. There are two quite separate senses in which phase evolutions and molecular dynamics may be considered to be correlated or uncorrelated. First, in the most stringent sense, the positions of all spin-bearing molecules may be strictly correlated between the first and second gradient pulse pairs. This would be the case, for example, when the pairs were applied in such rapid succession that molecules had not had a chance to move significantly, so that the position of a molecule at the end of the first pair became the position of the molecule at the beginning of the second. That is the special case dealt with in Section 8.6. But there is a weaker sense of correlation of equal interest, even if molecules have moved significantly over a time interval (the so-called mixing time) that may intervene between the application of the two pulse pairs. The positions of the molecules are now uncorrelated, but provided that they retain the same 'local properties', each molecular-borne spin gains a successive phase shift specific to those individualised properties. For example, if by 'local property' we mean confined to an anisotropic pore or domain, such that any resulting anisotropic translational motion will cause a phase response dependent on the direction of the applied gradient, then we will find that the relative directions of the gradients in the two pulse pairs becomes highly significant.

8.5.2 The propagator description $\tau_m \gg a^2/D$

A clearer understanding of the effect of the double wavevector encoding arises from a use of a propagator description in the narrow gradient pulse approximation. A general version of the pulse sequence is shown in Fig. 8.11. The echo attenuation resulting from this sequence may be written

$$E(\mathbf{q}_1,\mathbf{q}_2) = \iiiint P(\mathbf{r})\exp(i\mathbf{q}_1\cdot\mathbf{r})P(\mathbf{r}|\mathbf{r}',\Delta)\exp(-i\mathbf{q}_1\cdot\mathbf{r}') \times P(\mathbf{r}'|\mathbf{r}'',\tau_m)\exp(-i\mathbf{q}_2\cdot\mathbf{r}'')P(\mathbf{r}''|\mathbf{r}''',\Delta)\exp(i\mathbf{q}_2\cdot\mathbf{r}''')d\mathbf{r}d\mathbf{r}'d\mathbf{r}''d\mathbf{r}''' \quad (8.35)$$

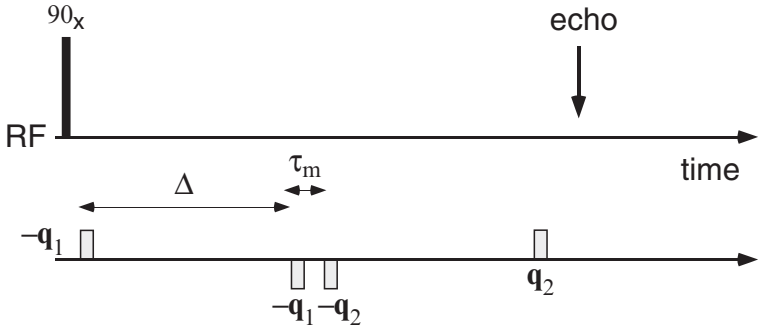

Fig. 8.11 Schematic RF and gradient pulse sequences for a general double wavevector encoding in which the PGSE pairs are represented by wavevectors $\mathbf{q}_1$ and $\mathbf{q}_1$, which may have independent directions.

Let us first deal with the case of free diffusion, where the propagator is always the Gaussian $P(\mathbf{r}|\mathbf{r}',t) = (4\pi Dt)^{-3/2}\exp(-(\mathbf{r}'-\mathbf{r})^2/4Dt)$, and

$$\begin{aligned} E(\mathbf{q}_1,\mathbf{q}_2) = \iiiint & P(\mathbf{r})\exp(-i\mathbf{q}_1\cdot(\mathbf{r}'-\mathbf{r}))(4\pi D\Delta)^{-3/2}\exp(-(\mathbf{r}'-\mathbf{r})^2/4D\Delta) \\ & \times(4\pi D\tau_m)^{-3/2}\exp(-(\mathbf{r}''-\mathbf{r}')^2/4D\tau_m) \\ & \times\exp(i\mathbf{q}_2\cdot(\mathbf{r}'''-\mathbf{r}''))(4\pi D\Delta)^{-3/2}\exp(-(\mathbf{r}'''-\mathbf{r}'')^2/4D\Delta)d\mathbf{r}d\mathbf{r}'d\mathbf{r}''d\mathbf{r}''' \\ = & \exp(-(q_1^2+q_2^2)D\Delta) \end{aligned} \tag{8.36}$$

This experiment is equivalent to simply multiplying the attenuations obtained from two separate single PGSE experiments carried out with different wavevectors. It contains no new information.

Next we consider what happens when the diffusion is restricted, such that $\Delta \gg a^2/D$ but the mixing time is also sufficiently long, $\tau_m \gg a^2/D$, that restricted diffusion is experienced over τ_m. For each interval, the propagator reduces to $\rho(\mathbf{r})$, so that

$$\begin{aligned} E(\mathbf{q}_1,\mathbf{q}_2) = & \iiiint P(\mathbf{r})\exp(i\mathbf{q}_1\cdot\mathbf{r})\rho(\mathbf{r}')\exp(-i\mathbf{q}_1\cdot\mathbf{r}') \\ & \times\rho(\mathbf{r}'')\exp(-i\mathbf{q}_2\cdot\mathbf{r}'')\rho(\mathbf{r}''')\exp(i\mathbf{q}_2\cdot\mathbf{r}''')d\mathbf{r}d\mathbf{r}'d\mathbf{r}''d\mathbf{r}''' \\ = & \left|\int\rho(\mathbf{r})\exp(i\mathbf{q}_1\cdot\mathbf{r})d\mathbf{r}\right|^2\left|\int\rho(\mathbf{r})\exp(i\mathbf{q}_2\cdot\mathbf{r})d\mathbf{r}\right|^2 \\ = & |\tilde{\rho}(\mathbf{q}_1)|^2|\tilde{\rho}(\mathbf{q}_2)|^2 \end{aligned} \tag{8.37}$$

where $\tilde{\rho}(\mathbf{q})$ is the pore spectral density. Again, we might be tempted to believe that the experiment is equivalent to simply multiplying the attenuations obtained from two separate single PGSE experiments. However, this is not quite the case. New information is present when the pores are locally anisotropic, because the effect of successive wavevectors of different orientation must be calculated for each pore. The derivation is subtle, and most easily worked out in the low-q limit. We will work to fourth order (q^4) and so expand $\tilde{\rho}(\mathbf{q})$ as

$$\begin{aligned} \tilde{\rho}(\mathbf{q}) = 1 & - i\int d\mathbf{r}(\mathbf{q}\cdot\mathbf{r})\rho(\mathbf{r}) - \tfrac{1}{2}\int d\mathbf{r}(\mathbf{q}\cdot\mathbf{r})^2\rho(\mathbf{r}) \\ & -i\tfrac{1}{6}\int d\mathbf{r}(\mathbf{q}\cdot\mathbf{r})^3\rho(\mathbf{r}) + \tfrac{1}{24}\int d\mathbf{r}(\mathbf{q}\cdot\mathbf{r})^4\rho(\mathbf{r}) + \mathcal{O}(q^6) + ... \end{aligned} \tag{8.38}$$

The problem is greatly simplified if we allow for inversion symmetry in $\rho(\mathbf{r})$, in which case all the odd powers disappear and

$$|\tilde{\rho}(\mathbf{q}_1)|^2|\tilde{\rho}(\mathbf{q}_2)|^2 = 1 - \int d\mathbf{r}(\mathbf{q}_1\cdot\mathbf{r})^2\rho(\mathbf{r}) - \int d\mathbf{r}(\mathbf{q}_2\cdot\mathbf{r})^2\rho(\mathbf{r}) + \tfrac{1}{12}\int d\mathbf{r}(\mathbf{q}_1\cdot\mathbf{r})^4\rho(\mathbf{r}) + \tfrac{1}{12}\int d\mathbf{r}(\mathbf{q}_2\cdot\mathbf{r})^4\rho(\mathbf{r}) + \tfrac{1}{4}\left[\int d\mathbf{r}(\mathbf{q}_1\cdot\mathbf{r})^2\rho(\mathbf{r})\right]^2 + \tfrac{1}{4}\left[\int d\mathbf{r}(\mathbf{q}_2\cdot\mathbf{r})^2\rho(\mathbf{r})\right]^2 + \int d\mathbf{r}(\mathbf{q}_1\cdot\mathbf{r})^2\rho(\mathbf{r})\int d\mathbf{r}(\mathbf{q}_2\cdot\mathbf{r})^2\rho(\mathbf{r}) + \mathcal{O}(q^6) + ... \tag{8.39}$$

Now let us address the case where there exists an ensemble of pores, each labelled by j. Then eqn 8.37 must be rewritten

$$E(\mathbf{q}_1,\mathbf{q}_2) = \frac{1}{N}\sum_j^N |\tilde{\rho}_j(\mathbf{q}_1)|^2|\tilde{\rho}_j(\mathbf{q}_2)|^2 \tag{8.40}$$

We will see in the next section that the anisotropy to which the double wavevector experiment is sensitive provides a characteristic signal that survives the effect of the ensemble sum.

8.5.3 Local anisotropy, global isotropy

Equation 8.39 involves a correlation of local diffusion along differing relative directions, even though the final average may be taken over all pore orientations. Thus the measurement has an inherent capacity to reveal local pore or diffusion anisotropy, even when the global polydomain structure is isotropic. The way in which this may be analysed has followed two alternative approaches. In the first, due to Cheng and Cory [16], the problem is treated by developing eqn 8.39 as a case of restricted diffusion in isolated pores the shape of which is described by an ellipsoid of revolution, as shown in Fig. 8.12(a). Figure 8.12(b) and (c) present an alternative description in which diffusion is long range but the local diffusion coefficient is anisotropic, as might be found in polydomain lyotropic liquid crystals.

We will deal first with the restricted pore diffusion approach. Suppose we assign $\mathbf{q}_1$ and $\mathbf{q}_2$ the same magnitude q, but with different polar angles with respect to $\mathbf{r}$, θ_1, and θ_2. In eqn 8.39, each term $\mathbf{q}_1\cdot\mathbf{r}$ is replaced with $qr\cos\theta_1$. Next we allow for all pore orientations by averaging over the ensemble as indicated in eqn 8.40, writing $\frac{1}{N}\sum_j^N = \langle ... \rangle$. Each pore might have some characteristic 'director' expressing its orientation. By way of example, for a pore comprising an ellipsoid of revolution, this director might be the long axis. Clearly, for an isotropic distribution of pore directors, where all possible relative orientations of pore and gradient wavevector are equally allowed, any axis is a suitable polar axis with which to calculate the orientational average of all pore responses. Hence integrals involving a single value of θ are identical, and we may rewrite eqn 8.39 as

$$E(\mathbf{q}_1,\mathbf{q}_2) = 1 - 2q^2\left\langle \int d\mathbf{r}\cos^2\theta_1 r^2\rho(\mathbf{r})\right\rangle + \tfrac{1}{6}q^4\left\langle \int d\mathbf{r}\cos^4\theta_1 r^4\rho(\mathbf{r})\right\rangle$$
$$+\tfrac{1}{2}q^4\left\langle \left[\int d\mathbf{r}\cos^2\theta_1 r^2\rho(\mathbf{r})\right]^2\right\rangle$$
$$+q^4\left\langle \iint d\mathbf{r}d\mathbf{r}'\cos^2\theta_1 r^2\rho(\mathbf{r})\cos^2\theta_2 r'^2\rho(\mathbf{r}')\right\rangle + \mathcal{O}(q^6) + ...$$
(8.41)

For pores where $\rho(\mathbf{r})$ is anisotropic, the third term in q^4 contains an integral that depends on the relative orientation of the gradients and the shape of the pore. In particular, that integral has an angular weighting $[\cos^2(\theta_1+\theta_2)+\cos^2(\theta_1-\theta_2)+2\cos(\theta_1-\theta_2)\cos(\theta_1+\theta_2)]$. The isotropic averaging[3] causes the the third trigonometric term in the square brackets to be zero. However, the second term in the square brackets is non-zero for anisotropic pores and has a coefficient $\cos^2\Theta$, where $\Theta = (\theta_1-\theta_2)$, the fixed angle between the two gradient pulses. Thus, it is the this $\cos^2\Theta$ term that determines the echo-attenuation dependence on the relative orientation of the pulses. Clearly, the greatest difference arises for $\Theta = 0$ and $\Theta = 90°$. The best means of revealing the pore anisotropy will be to carry out two experiments, with the two pairs of gradient pulses collinear or orthogonal. The corresponding echo attenuations are labelled $E_{zz}(q)$ and $E_{zx}(q)$.

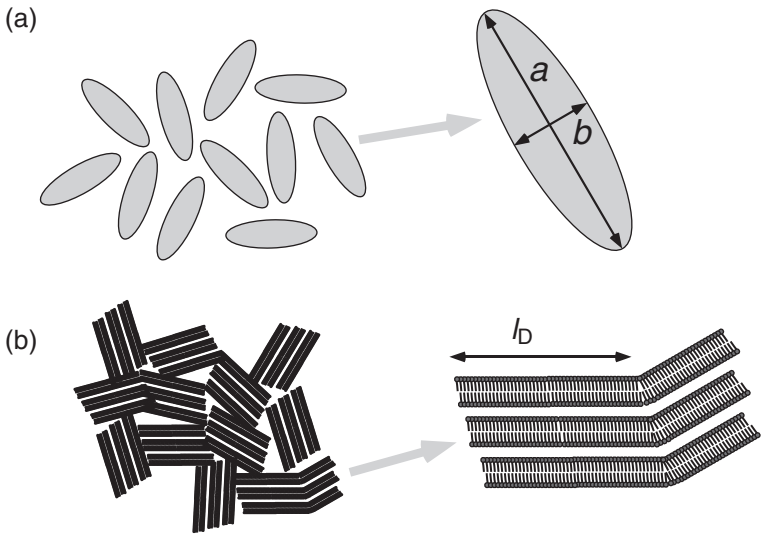

Fig. 8.12 (a) Array of ellipsoidal pores in which diffusion is restricted. The pores are randomly oriented but have a characteristic local anisotropy. (b) Polydomain lamellar lyotropic liquid crystals in which the domains are randomly oriented but have a characteristic local diffusion anisotropy.

[3]i.e. allowing θ_1 and θ_2 to independently vary over all polar angles.

Restricted diffusion in ellipsoidal pores

The analysis of Cheng and Cory for ellipsoidal pores leads to the result

$$\begin{aligned} E_{zz}(q) &= 1 - c_2 q^2 + c_4 q^4 + \mathcal{O}(q^6) + ... \\ E_{zx}(q) &= 1 - d_2 q^2 + d_4 q^4 + \mathcal{O}(q^6) + ... \end{aligned} \tag{8.42}$$

where

$$\begin{aligned} c_2 = d_2 &= \frac{2}{5}\left(\frac{2}{3}a^2 + \frac{1}{3}b^2\right) \\ c_4 - d_4 &= \frac{2}{375}\left(a^2 - b^2\right)^2 \end{aligned} \tag{8.43}$$

The local anisotropy effect occurs at fourth order in q and, of course, disappears for a sphere where $a = b$. This effect has been nicely demonstrated in a double wavevector restricted diffusion experiment on yeast cells, as shown in Fig. 8.13. The data are fitted to a polynomial, and the value c_2 and difference in the quadratic terms $c_4 - d_4$ are used to fix the ellipsoidal semi-axes at 13 and 2.2 microns for a and b.

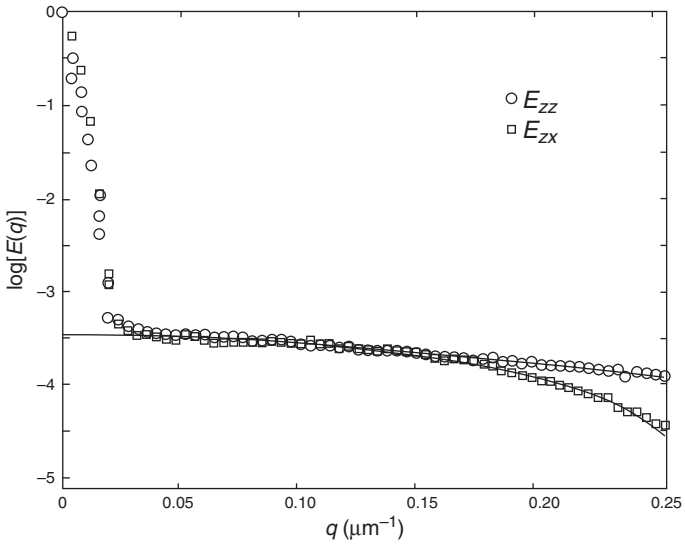

Fig. 8.13 Double PGSE NMR spin-echo-attenuation data curves for yeast cells. The open circles and squares correspond to parallel and perpendicular scattering vectors, respectively. The solid lines are fitted to a power series with seven terms. In these experiments the gradient pulse length was 1.0 ms, $\Delta = 40$ ms, and $\tau_m = 40$ ms. (Adapted from Cheng and Cory [16].)

General expression for anisotropic pores

Lawrenz *et al.* [17] have derived a general fourth order echo-attenuation expression for anisotropic pores in the long mixing time limit. Defining the moment

$R_{jk} = \int_{pore} \rho(\mathbf{r}) r_i r_j d\mathbf{r}$, they find that the double wavevector echo attenuation when $q_1 = q_2 = q$ and the angle between the gradients is Θ, is given by

$$\begin{aligned} E(q,\Theta) = 1 &- \tfrac{2}{3}\left\langle r^2 \right\rangle q^2 \\ &+ \frac{1}{10}\left[\left\langle r^4 \right\rangle + \sum_k R_{kk}^2 + \sum_{k\neq l} R_{kk}R_{ll}\right] q^4 \\ &+ \frac{1}{30}\left[\sum_k R_{kk}^2 - \sum_{k\neq l} R_{kk}R_{ll}\right] cos(2\Theta) q^4 + O(q^6) + ... \end{aligned} \tag{8.44}$$

This equation reproduces the result for ellipsoids of revolution given in eqn 8.43. But it also tells us that the angular effect at long mixing times first appears in the q^4 term, and always with an angular dependence $\cos 2\Theta$. Hence the biggest difference in echo attenuations will be between $\Theta = 0$ and $\Theta = \pi/2$.

Locally anisotropic diffusion with ellipsoidal symmetry

In the example shown in Fig. 8.12(b) a different approach is required. Here the use of a locally anisotropic diffusion coefficient allows the calculation of the echo attenuation for the separate cases of E_{zz} and E_{zx}. The method of analysis [18] follows that of Section 6.6.3 and, as for eqn 6.89, assumes that the diffusing molecules remain in their starting domains. In other words, $l_D^2 \gg D\Delta$. For polydomain lamellar liquid crystals the symmetry is such that $D_\perp \gg D_\parallel$ and $D_\perp \approx D_0$, the free molecular self-diffusion coefficient. However, for any $D_\perp$, $D_\parallel$, one obtains the relations

$$\begin{aligned} E_{zz}(q) &= \int_0^1 \exp(-q^2\Delta[2D_\parallel x^2 + 2D_\perp(1-x^2)])dx \\ E_{zx}(q) &= (2\pi)^{-1}\int_0^{2\pi}\int_0^1 \exp(-q^2\Delta[D_\parallel x^2 + D_\parallel(1-x^2)\cos^2\phi + D_\perp(1-x^2) \\ &\quad + D_\perp \sin^2\phi + D_\perp x^2\cos^2\phi])d\phi dx \end{aligned} \tag{8.45}$$

Expanding these expressions as power series to q^4 gives

$$\begin{aligned} E_{zz}(q) &= 1 - q^2\Delta[\tfrac{2}{3}D_\parallel + \tfrac{4}{3}D_\perp] \\ &\quad + \tfrac{1}{2}q^4\Delta^2[\tfrac{12}{15}D_\parallel^2 + \tfrac{16}{15}D_\perp D_\parallel + \tfrac{32}{15}D_\perp^2] + \mathcal{O}(q^6) + ... \\ E_{zx}(q) &= 1 - q^2\Delta[\tfrac{2}{3}D_\parallel + \tfrac{4}{3}D_\perp] \\ &\quad + \tfrac{1}{2}q^4\Delta^2[\tfrac{8}{15}D_\parallel^2 + \tfrac{24}{15}D_\perp D_\parallel + \tfrac{28}{15}D_\perp^2] + \mathcal{O}(q^6) + ... \end{aligned} \tag{8.46}$$

Note that as in the previous example, where restricted diffusion in elliptical pores was assumed, the difference between the $E_{zz}(q)$ and $E_{zx}(q)$ attenuations shows up only to fourth order in q. To use the language of the previous example,

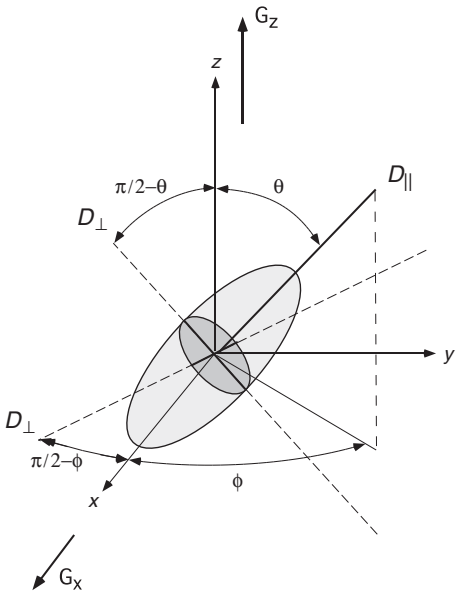

Fig. 8.14 Schematic showing the polar geometry of a randomly oriented locally anisotropic diffusion domain. Cylindrical symmetry is assumed and one of the two $D_\perp$ axes is chosen to be normal to the z direction.

$$c_2 = d_2 = \Delta[\tfrac{2}{3}D_\parallel + \tfrac{4}{3}D_\perp]$$
$$c_4 - d_4 = \tfrac{2}{15}\Delta^2[D_\parallel - D_\perp]^2 \tag{8.47}$$

Again, local isotropy causes the difference in q^4 terms to disappear. Note that for for all relative values of $D_\parallel$ and $D_\perp$ where these two differ, we always find that the echo attenuation for E_{zx} is greater than for E_{zz}. The reason for this universal effect can be found in the much greater proportion of solid angle available when the polar angle is close to the equator. What eqn 8.47 tells us is that a pulse sequence in which the two gradient pairs have their directions switched between orthogonal orientations will always optimise the proportion of spins with displacements close to the gradient directions. The same universality holds true in the case of restricted diffusion in anisotropic pores, as is evident in the sign independence of $c_4 - d_4$ on the prolate or oblate character of the ellipsoidal pore.

One simple example of a system in which diffusion is locally anisotropic but globally isotropic is provided by a polydomain lyotropic liquid crystal in the lamellar phase. Here the bilayers impede water diffusion normal to the lamellae, while diffusion is relatively free within the intervening aqueous layers. This is an example of 2-D anisotropy in which $D_\parallel = 0$ and $D_\perp = D$. Figure 8.15 shows results obtained using collinear (E_{zz} and E_{xx}) and orthogonal (E_{zx} and E_{xz}) encoding directions for water diffusing in the polydomain lamellar phase of Aerosol OT/water [19]. This system has been shown by X-ray diffraction experiments [20] to have a lamellar spacing of around 10 nm, at a distance diffused by a water molecule over a time of around 0.025 ms. In the typical PGSE observation times, Δ, of several milliseconds, water molecules will freely diffuse

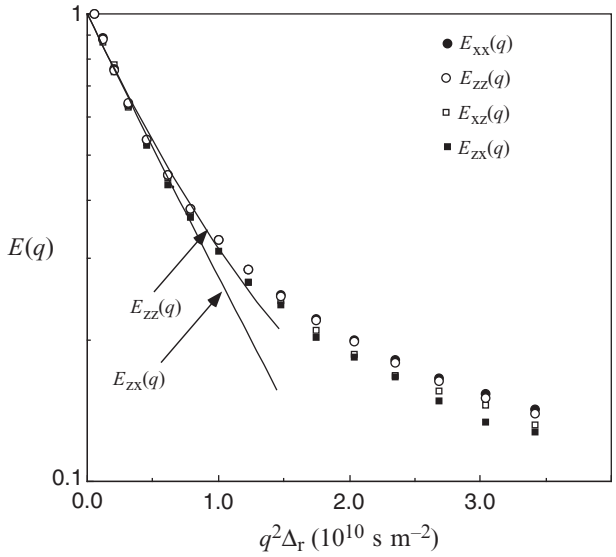

Fig. 8.15 Comparison of echo attention obtained using collinear (E_{zz} and E_{xx}) and orthogonal (E_{zx} and E_{xz}) encoding directions, for water diffusing in the polydomain lamellar phase of Aerosol OT/water. A difference is found in the echo attenuations in the collinear and orthogonal cases, indicating local anisotropy. The theoretical lines are based on eqn 8.45 and fitting the water diffusion coefficient from the initial slope of the data. (Reproduced from reference [18].)

in the $\perp$ directions in the water planes sandwiching the bilayers, the diffusion appearing unrestricted in these directions while effectively zero along the bilayer normals. However, previous experiments suggest domain sizes of around 10 to 15 μm that are traversed only for diffusion observation times of 50 ms or greater, so that values of Δ on the order of 10 ms, as used in the measurements shown in Fig. 8.15, should ensure that water molecules are confined to a single local domain.

The lamellar phase of Aerosol OT is known to be strongly influenced by defect structures and micellar inclusions, which impede free water diffusion along the layers [21]. In the quantitative fit to the data shown in Fig. 8.15, the water diffusion coefficient is 2 x 10^{-10} m^2 s^{-1}, an order of magnitude smaller than for free water. These defects may also explain why the observed ratio between E_{zz} and E_{zx} is less than predicted by eqn 8.47. Nonetheless, the signal difference between collinear and orthogonal double wavevector encoding is apparent.

8.6 Restricted diffusion and double wavevector encoding with infinitesimal mixing

The behaviour of the double wavevector echo attenuation in the case where molecules are restricted to pores becomes quite extraordinary when the mixing time is made to be short, a phenomenon first recognised by Mitra in 1995 [22]. The behaviour is not

only paradoxical, but it is also extremely useful, especially when one seeks to elucidate diffusive diffraction effects in disordered systems.

8.6.1 The Mitra paradox

Some physical insight can be obtained by analysing the effect of the double PGSE NMR sequence of Fig. 8.16, where two special cases of are illustrated, both of which have the mixing time τ_m between the pairs much shorter than the characteristic time τ_c to diffuse across a pore. For the purposes of this argument $\tau_m = 0$.

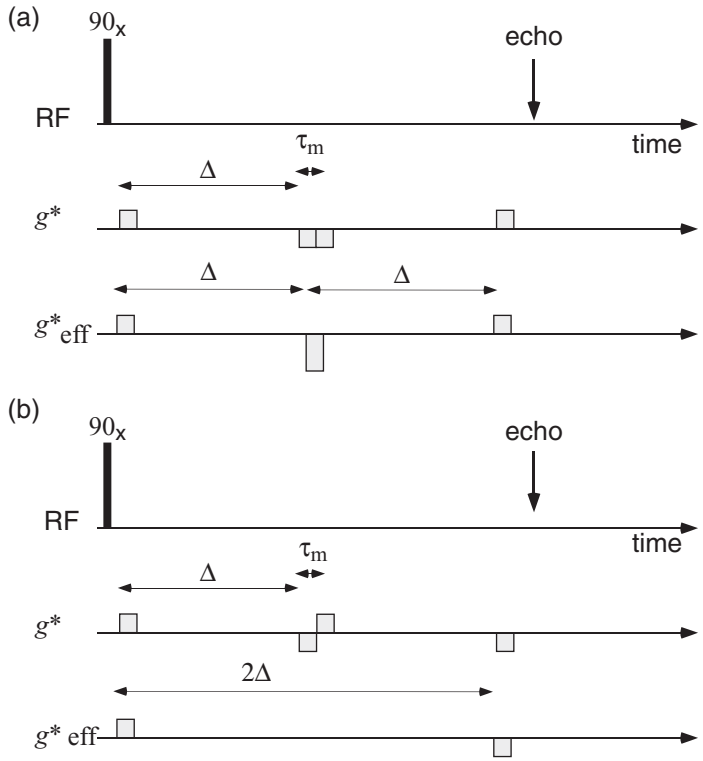

Fig. 8.16 Schematic RF and co-directional gradient pulse sequences for double wavevector encoding using two pairs of gradient pulses applied in quick succession such that the mixing time τ_m is much less that the characteristic time to diffuse across a pore, τ_c. In (a) the pulse pairs have opposite sense, while in (b) they have the same sense. In this latter case the second pulse from the first pair cancels the first from the second pair.

In Fig. 8.16(a), the pairs of gradient pulses are collinear and applied in opposite sense. In (b) they are applied in the identical sense and in consequence the second pulse of the first pair cancels the first pulse of the second pair. The net result is that (a) represents two successive encodings with encoding time Δ, while (b) represents a single encoding pair, but with encoding time 2Δ. Consider first the case of free diffusion, or alternatively $\Delta \ll \tau_c$. In (a), the motions of the molecules in the first

and second encoding periods Δ are completely uncorrelated. Both the first and second pulse pairs produce an attenuation $\exp(-q^2D\Delta)$, such that resulting echo attenuation is $\exp(-2q^2D\Delta)$. In (b), the single pulse pair results in attenuation $\exp(-q^2D2\Delta)$. The outcomes of (a) and (b) are identical.

By contrast, consider the case of restricted diffusion, $\Delta \gg \tau_c$. In (b) the equivalent single pulse pair results in attenuation $|S(q)|^2$, but in (a), a rather subtle effect ensues. We might be tempted to argue that the motions of the molecules in the first and second encoding periods Δ are again completely uncorrelated, so that both the first and second pulse pairs produce an attenuation $|S(q)|^2$, resulting in an overall echo attenuation $|S(q)|^4$. The outcomes of (a) and (b) would certainly be quite different. But the $|S(q)|^4$ outcome applies only when the mixing time is long. At infinitesimal mixing, the correlation of molecular positions at the end of the first and start of the second pulse pair requires a more careful analysis. Next we will see how the result may be exactly derived, and for any relative gradient orientations.

8.6.2 Propagator description, $\tau_m \ll a^2/D$

If $\tau_m \ll a^2/D$, the molecules have had insufficient time to change their displacements relative to the local pore geometry, and so we can represent that condition by setting the propagator for the mixing interval to a delta function. Hence eqn 8.37 must be rewritten

$$\begin{aligned}
E(\mathbf{q}_1,\mathbf{q}_2) &= \iiiint P(\mathbf{r})\exp(i\mathbf{q}_1\cdot\mathbf{r})\rho(\mathbf{r}')\exp(-i\mathbf{q}_1\cdot\mathbf{r}') \\
&\quad \times\delta(\mathbf{r}''-\mathbf{r}')\exp(-i\mathbf{q}_2\cdot\mathbf{r}'')\rho(\mathbf{r}''')\exp(i\mathbf{q}_2\cdot\mathbf{r}''')d\mathbf{r}d\mathbf{r}'d\mathbf{r}''d\mathbf{r}''' \\
&= \iiint P(\mathbf{r})\exp(i\mathbf{q}_1\cdot\mathbf{r})\rho(\mathbf{r}')\exp(-i\mathbf{q}_1\cdot\mathbf{r}') \\
&\quad \times\exp(-i\mathbf{q}_2\cdot\mathbf{r}')\rho(\mathbf{r}''')\exp(i\mathbf{q}_2\cdot\mathbf{r}''')d\mathbf{r}d\mathbf{r}'d\mathbf{r}''' \\
&= \int \rho(\mathbf{r})\exp(i\mathbf{q}_1\cdot\mathbf{r})d\mathbf{r}\int \rho(\mathbf{r}''')\exp(i\mathbf{q}_2\cdot\mathbf{r}''')d\mathbf{r}''' \\
&\quad \times\int \rho(\mathbf{r}')\exp(-i[\mathbf{q}_1+\mathbf{q}_2]\cdot\mathbf{r}')d\mathbf{r}' \\
&= \tilde{\rho}(\mathbf{q}_1)\tilde{\rho}(\mathbf{q}_2)\tilde{\rho}^*(\mathbf{q}_1+\mathbf{q}_2)
\end{aligned} \tag{8.48}$$

It is interesting to evaluate the prediction of eqn 8.48 along the lines of eqn 8.39. Again, we will assume pores with inversion symmetry, and this time work in the low-q limit and evaluate up to second order (q^2) to obtain

$$\begin{aligned}
\tilde{\rho}(\mathbf{q}_1)\tilde{\rho}(\mathbf{q}_2)\tilde{\rho}^*(\mathbf{q}_1+\mathbf{q}_2) = 1 &- \tfrac{1}{2}\int d\mathbf{r}(\mathbf{q}_1\cdot\mathbf{r})^2\rho(\mathbf{r}) + \tfrac{1}{2}\int d\mathbf{r}(\mathbf{q}_2\cdot\mathbf{r})^2\rho(\mathbf{r}) \\
&-\tfrac{1}{2}\int d\mathbf{r}((\mathbf{q}_1+\mathbf{q}_2)\cdot\mathbf{r})^2\rho(\mathbf{r}) + \mathcal{O}(q^4) + ...
\end{aligned} \tag{8.49}$$

Suppose we express eqn 8.49 for the case of isotropic pores where the absolute direction of $\mathbf{q}$ is irrelevant. We will see that their relative direction does, however, turn

out to be of considerable importance. For convenience we will assume that the two parts of gradient pulses have equal magnitudes q, but with different directions given the different polar angles, θ_1 and θ_2, which the vector $\mathbf{r}$ makes with respect to $\mathbf{q}_1$ and $\mathbf{q}_2$. With respect to $\mathbf{q}_1 + \mathbf{q}_2$, the polar angle is θ_{12}. Finally, we set the angle between $\mathbf{q}_1$ and $\mathbf{q}_2$ as Θ. Using this notation

$$\begin{aligned} E(\mathbf{q}_1, \mathbf{q}_2) &= \tilde{\rho}(\mathbf{q}_1)\tilde{\rho}(\mathbf{q}_2)\tilde{\rho}^*(\mathbf{q}_1 + \mathbf{q}_2) \\ &= \left(1 - \tfrac{1}{2}q^2 \int \cos^2\theta_1 r^2 \rho(\mathbf{r}) d\mathbf{r} + \mathcal{O}(q^4) + ...\right) \\ &\quad \times \left(1 - \tfrac{1}{2}q^2 \int \cos^2\theta_2 r^2 \rho(\mathbf{r}) d\mathbf{r} + \mathcal{O}(q^4) + ...\right) \\ &\quad \times \left(1 - \tfrac{1}{2}q^2(2 + 2\cos\Theta) \int \cos^2\theta_{12} r^2 \rho(\mathbf{r}) d\mathbf{r} + \mathcal{O}(q^4) + ...\right) \end{aligned} \tag{8.50}$$

where θ_{12} is the angle between the symmetry axis and $\mathbf{q}_1 + \mathbf{q}_2$. Each of the integrals $\int \cos^2\theta r^2 \rho(\mathbf{r}) d\mathbf{r}$ are identical and, for the isotropic pore, is simply $\frac{1}{3}\langle r^2 \rangle$, where $\langle r^2 \rangle$ is the mean-squared radius of gyration of the pores, $\int r^2 \rho(\mathbf{r}) d\mathbf{r}$. Given that, eqn 8.50 becomes

$$\begin{aligned} E(\mathbf{q}_1, \mathbf{q}_2) &= 1 - \tfrac{1}{3}q^2 \langle r^2 \rangle (2 + \cos\Theta) + \mathcal{O}(q^4) + ... \\ &= 1 - \tfrac{1}{3}q^2 \langle r^2 \rangle \left(1 + 2\cos\frac{\Theta}{2}\right) + \mathcal{O}(q^4) + ... \end{aligned} \tag{8.51}$$

Given our definition in eqn 8.48, where the sign of the $\mathbf{q}_1$ and $\mathbf{q}_2$ vectors is determined by the first and second pulses of the pairs, respectively, the case of Fig. 8.16(a) corresponds to $\cos\Theta = 1$ and Fig. 8.16(b) to $\cos\Theta = -1$. Note that the angular dependence is now in the q^2 term, a point to which we shall return. Unlike the long mixing-time case, the greatest difference in echo attenuation occurs between $\Theta = 0$ and $\Theta = \pi$.

The spherical pore and pore sizing

For a sphere, $\langle r^2 \rangle = \frac{3}{5}a^2$. For the case $\cos\Theta = -1$, where the coinciding pulses of the two pairs cancel, $E(\mathbf{q}_1, \mathbf{q}_2) = 1 - \frac{1}{5}q^2a^2$, as found for the single pulse pair in Chapter 7. For $\cos\Theta = 1$, the attenuation is three times greater and $E(\mathbf{q}_1, \mathbf{q}_2) = 1 - \frac{3}{5}q^2a^2$. The fact that the outcome of the experiment depends on the relative orientation of the gradient pulse pairs, despite the fact that no pore anisotropy has been assumed, is indeed remarkable.

One immediate application of the double wavevector encoding is the elucidation of the size of compartments in complex heterogeneous materials such as biological tissue. The appearance of a $\cos\Theta$ angular dependence of the echo attenuation at q^2 indicates restricted diffusion at short mixing time. Most importantly, the coefficient of this term provides an estimate of pore size [22–24]. Figure 8.17 shows the result of a set of double PGSE NMR experiments carried out at different mixing times, in three samples comprising porcine spinal cord, water between acrylate beads, and a radish sample, where the pores sizes are successively increasing. In each case a *cos*Θ angular

dependence is seen. At mixing times long compared with the time to diffuse across the pore, the anisotropy attenuates, of course, most rapidly in the sample with smallest pore size. From the amplitude of the $E(q,\pi)/E(q,0)$ variation, estimates of the pore sizes can be made.

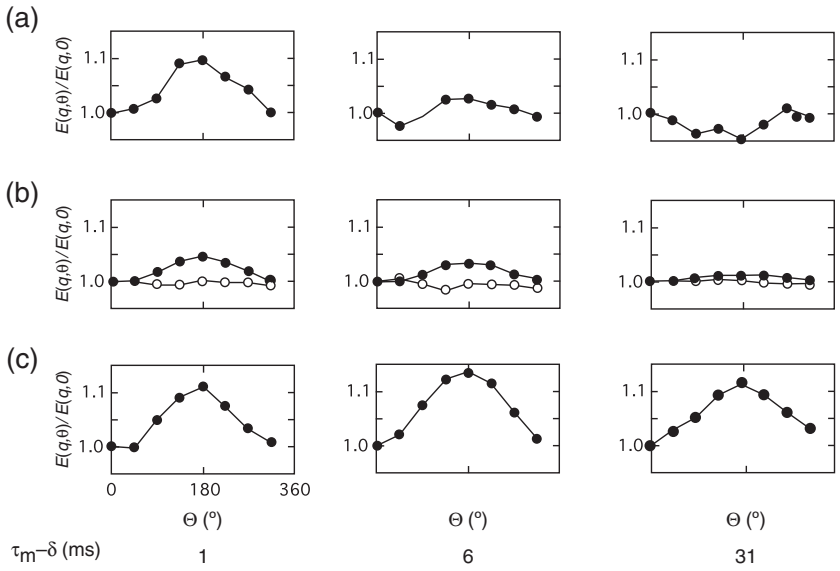

Fig. 8.17 Normalised signal versus Θ for different τ_m values, but at the same gradient pulse strength. (a) Porcine spinal cord ($\delta = 17$ ms), (b) water between acrylate beads ($\delta = 6$ ms) with the bulk water signal (open circles) shown for comparison, and (c) radish sample ($\delta = 6$ ms). The plots in each column share the value $\tau_m - \delta$=1, 6, and 31 ms (from left to right). Note that the q value is much greater for (a) because of the larger value of δ. The data have been fitted to yield pore sizes (radius a) estimates of 1.9, 4.1, and 7.4 microns, respectively for (a), (b), and (c). Note the absence of Θ dependence for the water sample and the gradual attenuation of the angular effect as the mixing time is increased. (Adapted from Koch and Finsterbusch [23].)

Note that the finite gradient pulse-width value, δ, presents some difficulty in the interpretation, not just because of the narrow gradient pulse approximation associated with the assignment of $\rho(\mathbf{r})$ to the propagator, but also because of uncertainty regarding the nature of the mixing time. However, these effects may be handled using the matrix multiple propagator methods described in Chapter 5. A detailed account of finite time effects using such methods has been given by Özarslan and Basser [25, 26].

Anisotropic pores

How does pore anisotropy reveal itself in the case of short mixing time? Certainly such anisotropy no longer permits the simple symmetry argument that led to eqn 8.51. Instead, eqn 8.49 yields

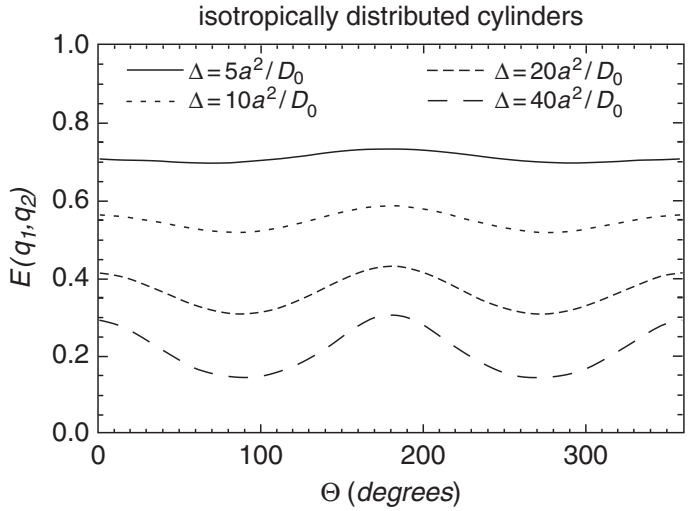

Fig. 8.18 Normalised double PGSE NMR signal from cylinders isotropically distributed in space showing echo attenuation E versus Θ for different Δ values, where $\tau_m = 0.002a^2/D_0$, $(\gamma\delta g a)^2 = 0.1$, and $\delta \to 0$. Note the onset of $\cos^2\Theta$ behaviour as the fourth-order terms appear at deeper attenuation. (Adapted from Özarslan and Basser [26].)

$$E(\mathbf{q}_1, \mathbf{q}_2) = 1 - q^2 \int \cos^2\theta_1 r^2 \rho(\mathbf{r}) d\mathbf{r} - q^2 \int \cos^2\theta_2 r^2 \rho(\mathbf{r}) d\mathbf{r} \\ -q^2(2 + 2\cos\Theta) \int \cos^2\theta_{12} r^2 \rho(\mathbf{r}) d\mathbf{r} + \mathcal{O}(q^4) + ... \qquad (8.52)$$

But even for anisotropic pores, an isotropic distribution means that any polar axis is suitable for an estimation of the orientational average response. The $1 + 2\cos^2(\Theta/2)$ dependence of the echo attenuation is the same as that observed for isotropic pores, although the coefficient $\left\langle \int \cos^2\theta_1 r^2 \rho(\mathbf{r}) d\mathbf{r} \right\rangle$ will be different, reflecting not only the size but also the shape of the pore. Nonetheless these is nothing in this coefficient that enables us to separate pore size and pore shape. To measure pore anisotropy, we need to include the q^4 term in the signal. Figure 8.18 shows the transition from $1 + 2\cos^2(\Theta/2)$ to $\cos^2(\Theta)$ behaviour, for an isotropic distribution of long cylinders, as the echo attenuation is increased and the fourth-order term comes into play. Hence the diffusion is restricted normal to the cylinder axis and free along the axis direction.

Figure 8.19, at much weaker attenuation, is dominated by the q^2 term and shows the requirement for very short mixing time in order to reveal the $1 + 2\cos^2(\Theta/2)$ dependence of the echo attenuation. As τ_m is increased to become comparable with the pore diffusion time, the angular dependence in the echo attenuation disappears. The calculation that allows an estimation of the echo attenuation for finite τ_m values [26] is described in the next section.

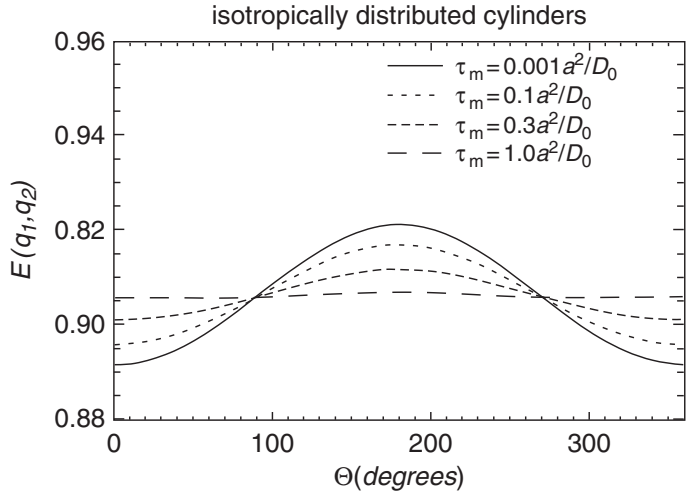

Fig. 8.19 Normalised double PGSE NMR signal from cylinders isotropically distributed in space, showing echo attenuation E versus Θ for different τ_m values, where $\Delta = a^2/D_0$, $(\gamma\delta g a)^2 = 0.1$, and $\delta \to 0$. Only the second-order (q^2) component of the echo attenuation is playing a role and the angular dependence disappears as the mixing time becomes longer. (Adapted from Özarslan and Basser [26].)

8.7 Restricted diffusion and double wavevector encoding with finite mixing time

8.7.1 First-order expression for restricted isotropic geometries with general pulse timings

Using the matrix multiple propagator method, and dividing the gradient waveform into M steps of duration τ and total time $T = M\tau$, Özarslan and Basser [26] have derived a general first-order (q^2) expression for the double wavevector experiment, applicable for all pulse timings. Their calculation involves a multiplication of $M \times M$ matrices [27], as outlined in Chapter 5. To assist the evaluation of the matrix multiplications of $S_k(\mathbf{q}) = V^{-1/2} \int d\mathbf{r} u_k(\mathbf{r}) \exp(i\mathbf{q_k} \cdot \mathbf{r})$ and $A_{kk'} = \int d\mathbf{r} u_k^*(\mathbf{r}) u_{k'}(\mathbf{r}) \exp(i\mathbf{q_{k'}} \cdot \mathbf{r})$, they define terms ${}_cA(\mathbf{q})$, and ${}_cS(\mathbf{q})$, which are proportional to $(\mathbf{q} \cdot \mathbf{r})^c$ in the Taylor series expansions. The integrals to be evaluated in order to find the coefficient of q^2 are then

$$ {}_2S^T(\mathbf{q}_i) R\ {}_0S^*(\mathbf{q}_j) = -\frac{1}{2V} \int_V d\mathbf{r} (\mathbf{q_i} \cdot \mathbf{r})^2 \tag{8.53} $$

and

$$ {}_1S^T(\mathbf{q}_i) R\ {}_1S^*(\mathbf{q}_j) = \frac{1}{V} \int_V d\mathbf{r} \mathbf{q_i} \cdot \mathbf{r} \int_V d\mathbf{r}' \mathbf{q_j} \cdot \mathbf{r}' P(\mathbf{r}|\mathbf{r}', t) \tag{8.54} $$

These terms depend on the shape of the pore. For planar, cylindrical, and spherical pores of plane spacing $2a$ or radii a, the results may easily be obtained in a closed form using the eigenmode expansions given in Chapter 7 as

$$ {}_2S^T(\mathbf{q}_i)R\ {}_0S^*(\mathbf{q}_j) = -\frac{\frac{1}{2}q_j^2a^2}{2+d} \tag{8.55} $$

and

$$ {}_1S^T(\mathbf{q}_i)R\ {}_1S^*(\mathbf{q}_j) = 2a^2\mathbf{q}_j \cdot \mathbf{q}_j \sum_{n=1}^{\infty} s_{dn}e^{-\alpha_{dn}^2 D_0(t_j-t_i)/a^2} \tag{8.56} $$

where d is the dimensionality 1, 2, or 3 appropriate to the plane, cylinder, or sphere, and the $\alpha_d n$ are, respectively, the roots σ_n, β_n, and α_n appropriate to the planar, cylinder, or sphere case as outlined in Chapter 7. s_{dn} is given by $[\alpha_{dn}^2(\alpha_{dn}^2 - d + 1)]^{-1}$. Allowing $M \to \infty$ and $\tau \to 0$, Özarslan and Basser derive the echo-attenuation expression to q^2 in terms of integrals over the effective gradient, $\mathbf{g}^*(t)$, as

$$ E \approx 1 - 2\gamma^2a^2 \sum_{n=1}^{\infty} s_{dn} \int dt e^{\alpha_{dn}^2 D_0 t/a^2} \mathbf{g}^*(t) \cdot \mathbf{F}_{dn}(t) \tag{8.57} $$

where

$$ \mathbf{F}_{dn}(t) = \int_t^T dt' \mathbf{g}^*(t) e^{-\alpha_{dn}^2 D_0 t'/a^2} \tag{8.58} $$

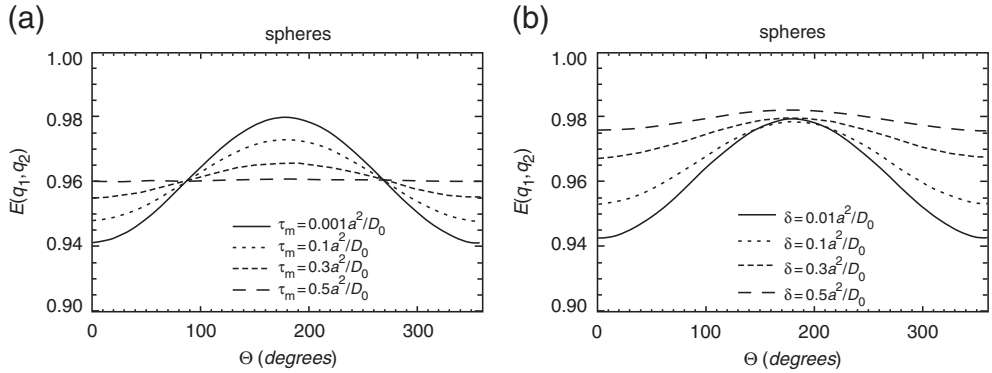

Fig. 8.20 Normalised double PGSE NMR signal from an ensemble of spheres, showing echo attenuation E versus Θ for (a) different τ_m values where $\Delta = a^2/D_0$, $(\gamma\delta g a)^2 = 0.1$, and $\delta \to 0$ and (b) different δ values where $\Delta = a^2/D_0$, $(\gamma\delta g a)^2 = 0.1$, and $\tau_m = 0.002a^2/D_0$. Only the second-order (q^2) component of the echo attenuation is playing a role, and the angular dependence disappears as the mixing time becomes longer, and as the increasing value of δ causes the experiment to approach the steady gradient case. (Adapted from Özarslan and Basser [26].)

Using these relations, the second-order echo-attenuation term can be calculated, in the case of plane pores, cylinders, or spheres, for any waveform whatsoever. Hence it is possible to examine how the angular dependence is perturbed by increasing the mixing time, or by increasing the gradient pulse duration δ. The results [26] are shown in Fig. 8.20. It is clear that the $1 + 2\cos^2(\Theta/2)$ dependence attenuates sharply as the mixing time becomes comparable with the time to diffuse across the pore, while in

the case where δ is varied, the approach to steady gradient conditions also results in a significant weakening of the angular dependence. Clearly, narrow gradient pulse and short mixing time conditions are ideal if the the angular dependence of the q^2 term in the echo attenuation is to be used to measure pore size. However, the finite time expressions at least permit the method to be used under a wider range of parameter space.

8.7.2 Isotropic fluid with unrestricted diffusion and finite width gradient pulse effects

There remains one other cautionary example to be considered in the matter of the angular dependence of differently aligned pulse pairs in double PGSE NMR. This curiosity concerns the case of an isotropic fluid undergoing free diffusion, where no Θ dependence would be expected. It arises when the double PGSE pulse sequence is implemented by superposing the last pulse of the first pair with the first pulse of the second pair, as shown in Fig. 8.21(b). In this case, the echo attenuation for two pulse pairs of magnetic field gradients g_1 and g_2 obeys [26]

$$E = \exp(-\gamma^2\delta^2 D_0[(\Delta - \delta/3)(g_1^2 + g_2^2) - (\delta/3)g_1 g_2 \cos\Theta]) \tag{8.59}$$

whereas the 'safer' pulse sequence shown in Fig. 8.21(a) returns the expected result

$$E = \exp(-\gamma^2\delta^2 D_0(\Delta - \delta/3)(g_1^2 + g_2^2) \tag{8.60}$$

The physical reason for this discrepancy is perfectly obvious. For the pulse sequence of Fig. 8.21(b), in the case $\Theta = 0$ we have to account for finite pulse-width effects in a three-pulse experiment, whereas when $\Theta = \pi$, the experiment is closer to a two-gradient pulse experiment.[4] By contrast, the sequence of Fig. 8.21(a) is always a four-gradient pulse experiment and the finite-width pulse sequence effects are proportionately the same for each pulse pair.

Because of this artifact, the pulse sequence of Fig. 8.21(a), with τ_m set as short as possible, should always be used for double PGSE NMR experiments targeted at measuring pore size through the angular dependence of the q^2 term in the echo attenuation. By this means one ensures that any observed angular dependence arises from signal contributions due to molecules experiencing restricted diffusion.

8.8 Diffusive diffraction with double PGSE NMR

Just as $|\tilde{\rho}(\mathbf{q}|^2$ is the PGSE NMR diffraction signal for the long-time limit ($\Delta \gg a^2/D_0$) for spin-bearing molecules diffusing in an enclosing pore, described by the density $\rho(\mathbf{r}$, then $|\tilde{\rho}(\mathbf{q}_1)|^2|\tilde{\rho}(\mathbf{q}_2)|^2$ and $\tilde{\rho}(\mathbf{q}_1)\tilde{\rho}(\mathbf{q}_2)\tilde{\rho}^*(\mathbf{q}_1+\mathbf{q}_2)$ are, respectively, the diffraction signals for double PGSE in the cases $\tau_m \gg a^2/D_0$ and $\tau_m \ll a^2/D_0$. As we have seen, the long mixing time case is of some interest where local anisotropy is to be examined in a system which is globally isotropic. But it is the case $\tau_m \ll a^2/D_0$ which arouses particular interest. In particular, unlike expressions for the long mixing time double

[4]It is precisely a two-pulse PGSE NMR experiment when $g_1 = g_2$ and $\Theta = \pi$.

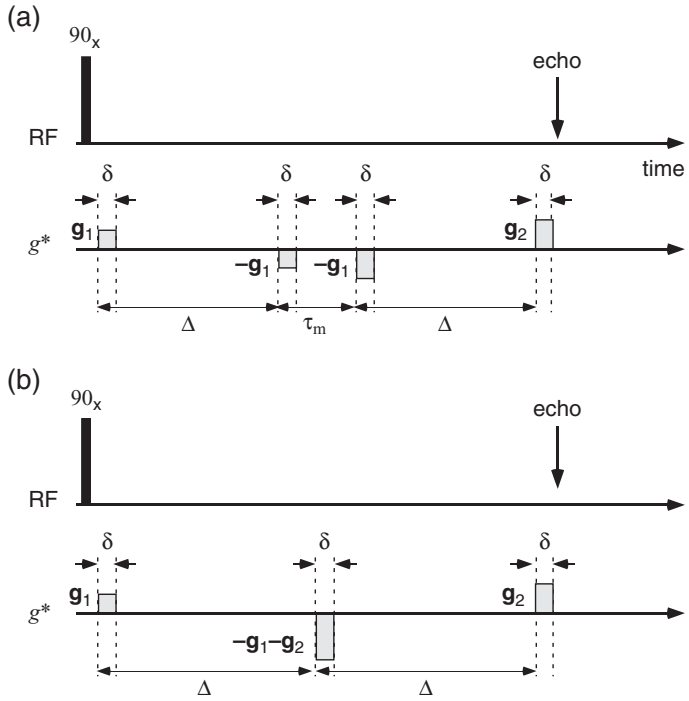

Fig. 8.21 Double PGSE NMR pulse sequences in which (a) the two pairs of gradient pulses are separate blocks separated by each other by an identifiable mixing time τ_m and (b) the last pulse of the first pair and the first pulse of the second pair are superposed so as to reduce τ_m. Sequence (b) can result in artifactual angular dependence due to finite pulse-width effects, even for a freely diffusing isotropic liquid. Pulse sequence (a) should be used to avoid these effects, even where tau_m is to be minimised. (Adapted from Özarslan and Basser [26].)

PGSE or single PGSE pair experiments, the short mixing time double PGSE NMR diffraction signal is not inherently positive. This enables far greater dynamic range in the signal and so can significantly aid the determination of structure.

8.8.1 Diffractograms with signed amplitude

Consider a multiple PGSE experiment in which N pairs of PGSE gradients, each of identical wavevector $\mathbf{q}$, are applied in succession such that in each case the diffusion time Δ is sufficiently long ($\Delta \gg a^2/D_0$) that molecules have diffused many time across the pore. In that case, a very simple form of the echo attenuation may be written down in the limit of long mixing times

$$E_{\infty,\infty}(\mathbf{q}, N) = |\tilde{\rho}(\mathbf{q})|^{2N} \tag{8.61}$$

where we follow reference [25] in using the double ∞ subscript to refer to conditions for Δ and τ_m. The diffraction signal is always positive.

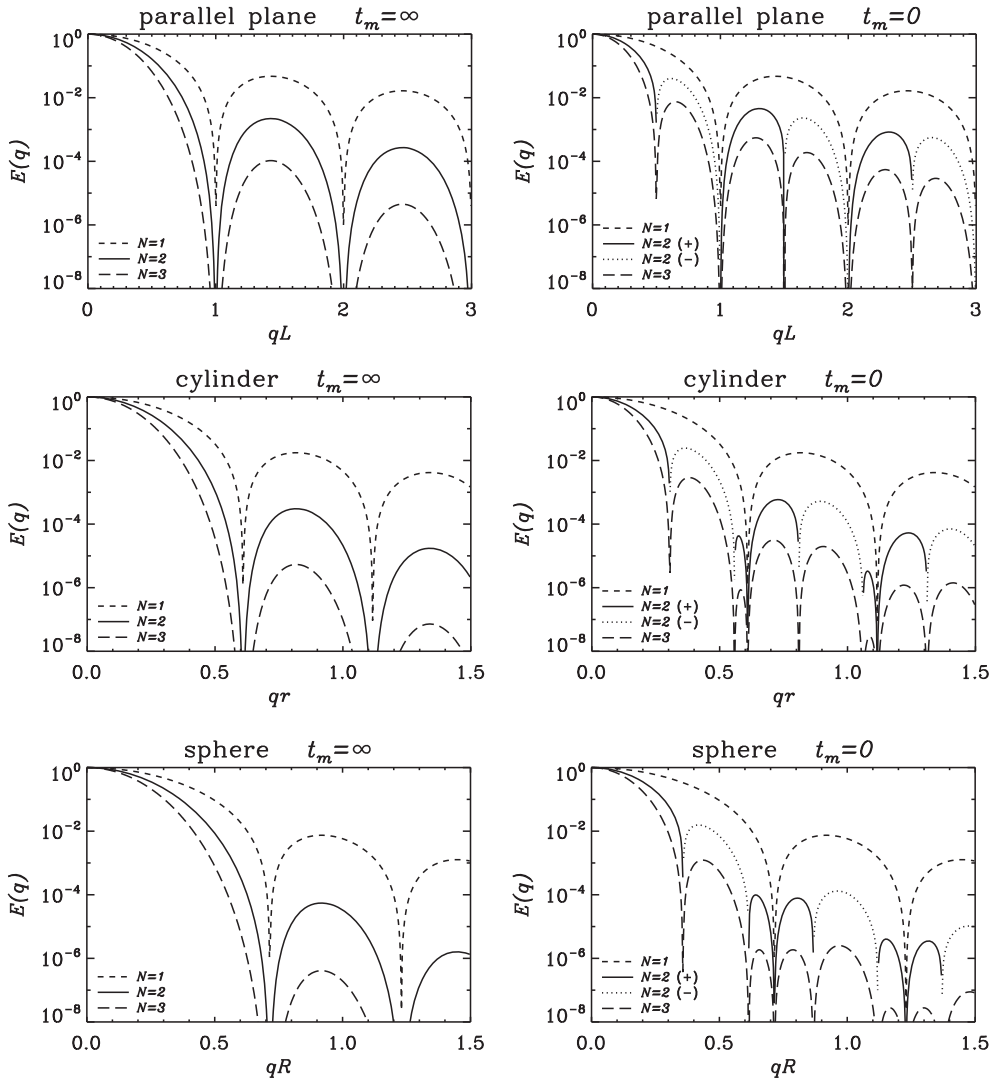

Fig. 8.22 Signal attenuation as a function of q with varying number of diffusion gradient pairs for parallel plane pore with spacing L (top), cylindrical pore with radius r (middle), and spherical pore with radius R (bottom). The left column shows the results obtained in the limit $\tau_m \to \infty$, while the $\tau_m = 0$ case is shown on the right column. In both cases $\delta \to 0$ and $\Delta_m \to \infty$. The continuous and dotted lines both illustrate the curve obtained with $N = 2$, where the former shows the positive sections and the latter shows the negative sections after flipping. (Reproduced from Özarslan and Basser [25].)

When the mixing time is short, signed diffraction signals may be obtained for even N. Following the simple reasoning above, one may write [25] for N odd

$$E_{\infty,0}(\mathbf{q}, N) = |\tilde{\rho}(\mathbf{q})|^2 |\tilde{\rho}(2\mathbf{q})|^{N-1} \tag{8.62}$$

while for N even

$$E_{\infty,0}(\mathbf{q}, N) = \tilde{\rho}(\mathbf{q})^2 \tilde{\rho}^*(2\mathbf{q}) |\tilde{\rho}(2\mathbf{q})|^{N-2} \tag{8.63}$$

Figure 8.22 shows the diffractograms for $N = 1, 2, 3$ in the case of planes separated by L, where the gradient is applied normal to the planes, cylinders of radius r, where the gradients are applied normal to the cylinder axis, and spheres of radius R. The right-hand set correspond to short mixing time and for $N = 2$, the dotted line indicates a signal of negative sign. In a sense, such a signed behaviour is merely a curiosity, and it is not obvious that greater information content is present. However, as we shall see in the next section, the importance of the signed oscillatory character of the $N = 2$ short mixing time diffraction signal is that it holds the key to unravelling structures: polydispersity.

8.8.2 Unravelling structure in polydisperse systems

Suppose our sample is made of spherical pores of differing radii. The result of the PGSE NMR experiment is a superposition of diffraction signals from each pore, each weighted by its probability in the distribution. Of course, what we would really like to do is to invert the data to obtain the distribution. Such an inversion is much simpler when the signals associated with each parameter of the distribution belongs to an orthogonal basis function. The real value of oscillatory signals is that they have the potential to provide just such an orthogonal basis.

Let us see how that might work with the three simple geometries of parallel planes, cylinders, and spheres, for which the structure factors, $\tilde{\rho}(\mathbf{q})$ are, respectively, $\sin(qa)/qa$, $J_1(qa)/qa$, and $j_1(qa)/qa$, a being the half-plane spacing, or the cylinder/sphere radius. We could take a pulse sequence similar to that shown in Fig. 8.21(b), where $g_1 = g_2 = g$, such that the superposed central pulse has amplitude $2gx$, where $x = \cos\Theta$. Then, for a distribution of pores sizes $P(a)$, the echo signal at a particular value of g and x would be

$$E_{\infty,0}(\mathbf{q}, x) = \int_0^\infty P(a) \tilde{\rho}(\mathbf{q})^2 \tilde{\rho}^*(2\mathbf{q}x) da \tag{8.64}$$

For convenience, choose the case of cylinders. Then

$$E_{\infty,0}(\mathbf{q}, x) = \int_0^\infty P(a) \left(\frac{J_1(qa)}{qa} \right)^2 \frac{J_1(2qxa)}{2qxa} da \tag{8.65}$$

This equation describes a 2-D experiment in which q and x may be independently varied. Given the Bessel function orthogonality [28],[5] then it follows for a particular q that

[5] $\int_0^\infty J_1(\alpha\rho) J_1(\alpha'\rho) \rho d\rho = \alpha^{-1} \delta(\alpha - \alpha')$.

$$P(a) = a^2 \left(\frac{J_1(qa)}{qa} \right)^{-2} F(a,q) \tag{8.66}$$

where

$$F(a,q) = \int_0^\infty E_{\infty,0}(\mathbf{q},x)(2qx)^2 J_1(2qxa) d(2qx) \tag{8.67}$$

the variable x being taken from 0 to 1, and the argument $2q$ being set large enough to sufficiently attenuate the echo when $x = 1$. Equations 8.66 and 8.67 are unfriendly to real experiments, where the $(2qx)^2$ factor in eqn 8.67 tends to emphasise the noise at high x values, while the static structure factor squared in eqn 8.66 causes poles in the division at the nodal points. Of course, by working with a sum of echo attenuations obtained at a few judiciously chosen q values, these poles may be avoided and, given good enough signal-to-noise in the experiment, the distribution $P(a)$ may be revealed.

References

[1] J. D. Seymour and P. T. Callaghan. Generalized approach to NMR analysis of flow and dispersion in porous media. *AIChE J.*, 43:2096, 1997.

[2] A. J. Sederman, M. L. Johns, P. Alexander, and L. F. Gladden. Structure-flow correlations in packed beds. *Chem. Eng. Sci.*, 53:2117, 1998.

[3] L. Lebon, L. LeBlond, and J. P. Hulin. Experimental measurement of dispersion processes at short times using a pulsed field gradient NMR technique. *Phys. Fluids*, 9:481, 1966.

[4] B. Manz, P. Alexander, and L. F. Gladden. Correlations between dispersion and structure in porous media probed by nuclear magnetic resonance. *Phys. Fluids*, 11:259, 1999.

[5] P. T. Callaghan and Y. Xia. Velocity and diffusion imaging in NMR microscopy. *J. Magn. Reson.*, 91:326, 1991.

[6] P. T. Callaghan, S. L. Codd, and J. D. Seymour. Spatial coherence phenomena arising from translational spin motion in gradient spin echo experiments. *Concepts in Magnetic Resonance*, 11:181, 1999.

[7] A. A. Khrapitchev and P. T. Callaghan. Reversible and irreversible dispersion in a porous medium. *Phys. Fluids*, 15:2649, 2003.

[8] G. I. Taylor. Dispersion of soluble matter in solvent flowing slowly through a pipe. *Proc. Roy. Soc. London A*, 219:186, 1953.

[9] A. A. Khrapitchev and P. T. Callaghan. Double PGSE NMR with stimulated echoes: phase cycles for the selection of desired encoding. *J. Magn. Reson.*, 152:1, 2001.

[10] M. W. Hunter and P. T. Callaghan. NMR measurement of nonlocal dispersion in complex flows. *Phys. Rev. Lett.*, 89:210602, 2007.

[11] M. W. Hunter, A. N. Jackson, and P. T. Callaghan. Nuclear magnetic resonance measurement and Lattice-Boltzmann simulation of nonlocal dispersion the tensor. *Phys. Fluids*, 22:027101, 2010.

[12] W. D. Williams, E. F. W. Seymour, and R. M. Cotts. A pulsed-gradient multiple-spin-echo NMR technique for measuring diffusion in the presence of background magnetic field gradients. *J. Magn. Reson.*, 31:271, 1978.

[13] R. Aris. On the dispersion of a solute in a fluid flowing through a tube. *Proc. Roy. Soc. A*, 235:67, 1956.
[14] C. Van Den Broeck. A stochastic description of longitudinal dispersion in uniaxial flows. *Physica A*, 112:343, 1982.
[15] D. G. Cory, A. N. Garroway, and J. B. Miller. Applications of spin transport as a probe of local geometry. *Polymer Preprints*, 31:149, 1990.
[16] Y. Cheng and D. G. Cory. Multiple scattering by NMR. *J. Am. Chem. Soc.*, 121:7935, 1999.
[17] M. Lawrenz, M. A. Koch, and J. Finsterbusch. A tensor model and measures of microscopic anisotropy for double-wave-vector diffusion-weighting experiments with long mixing times. *J. Magn. Reson.*, 202:43, 2010.
[18] P. T. Callaghan and M. E. Komlosh. Locally anisotropic motion in a macroscopically isotropic system: displacement correlations measured using double pulsed gradient spin echo NMR. *Magnetic Resonance in Chemistry*, 40:S15, 2002.
[19] J. Rogers and P. A. Winsor. Optically positive, isotropic and negative lamellar liquid crystalline solutions. *Nature*, 216:477, 1967.
[20] K. Fontell. The structure of the lamellar liquid crystalline phase in Aerosol OT–water system. *J. Colloid Interface Sci.*, 44:318, 1973.
[21] P. T. Callaghan and O. Söderman. Examination of the lamellar phase of Aerosol OT/water using pulsed field gradient nuclear magnetic resonance. *J. Phys. Chem.*, 87:1737, 1983.
[22] P. P. Mitra. Multiple wave-vector extensions of the NMR pulsed field gradient spin echo diffusion method. *Phys. Rev. B*, 51:15074, 1995.
[23] M. A. Koch and J. Finsterbusch. Compartment size estimation with double wave vector diffusion-weighted imaging. *Magn. Reson. Med.*, 60:90, 2008.
[24] N. Shemesh, E. Özarslan, P. J. Basser, and Y. Cohen. Measuring small compartmental dimensions with low-q angular double-PGSE NMR: The effect of experimental parameters on signal decay. *J. Magn. Reson.*, 198:15, 2009.
[25] E. Özarslan and P. J. Basser. MR diffusion–'diffraction' phenomenon in multi-pulse-field-gradient experiments. *J. Magn. Reson.*, 188:285, 2007.
[26] E. Özarslan and P. J. Basser. Microscopic anisotropy revealed by NMR double pulsed field gradient experiments with arbitrary timing parameters. *J. Chem. Phys.*, 128:158511, 2008.
[27] P. T. Callaghan. A simple matrix formalism for the spin echo analysis of restricted diffusion under generalised gradient waveforms. *J. Magn. Reson.*, 129:74, 1997.
[28] G. B. Arfken and H. J. Weber. *Mathematical Methods for Physicists*. Cambridge, New York, 2005.